Cellular Exposure to Chloroacetanilide Herbicides Induces Distinct Protein Destabilization Profiles

Guy M. Quanrud, Sunil V. Balamurugan, Carolina Canizal, and Joseph C. Genereux[*]

Department of Chemistry, University of California, Riverside, CA 92521

*Joseph C. Genereux, E-mail: josephg@ucr.edu

Abstract:

Herbicides in the popular chloroacetanilide class harbor a potent electrophilic moiety, which can damage proteins through nucleophilic substitution. In general, damaged proteins are subject to misfolding. Accumulation of misfolded proteins compromises cellular integrity by disrupting cellular proteostasis networks, which can further destabilize the cellular proteome. While direct conjugation targets can be discovered through affinity-based protein profiling, there are few approaches to probe how cellular exposure to toxicants impacts the stability of the proteome. We apply a quantitative proteomics methodology to identify chloroacetanilide-destabilized proteins in HEK293T cells based on their binding to the H31Q mutant of the human Hsp40 chaperone DNAJB8. We find that brief cellular exposure to the chloroacetanilides acetochlor, alachlor, and propachlor induces misfolding of dozens of cellular proteins. These herbicides feature distinct but overlapping profiles of protein destabilization, highly concentrated in proteins with reactive cysteine residues. Propachlor induces a general increase in protein aggregation, and selectively targets GAPDH and PARK7, leading to a decrease in their cellular activities. GAPDH is primarily modified by direct conjugation of propachlor at a catalytic cysteine residue, leading to global destabilization of the protein. The Hsp40 affinity strategy is an effective technique to profile cellular proteins that are destabilized by cellular toxin exposure.

Raw proteomics data is available through the PRIDE Archive at PXD030635.

Introduction:

Proteins contain numerous nucleophilic sites, including the cysteine thiol, the lysine ε-amine, and the N-terminus[1]. These reactive sites enable post-translational modifications that play central roles in cellular signaling and function, but protein nucleophiles are also subject to modification by environmental and metabolic electrophiles[2]. This damage can deprive the cell of protein function[3], interfere with binding interactions[4], or promote protein misfolding and toxic aggregation[5]. Despite the clear threat that electrophilic exposure agents present to the cellular proteome and protein homeostasis, protein conjugation by environmental toxicants is not nearly as well investigated as nucleic acid conjugation. This stems in part from the larger dynamic range for nucleophilicity in proteins as compared to nucleic acids[6]. Nucleic acid reactivities vary far less than protein reactivities, and the mutagenic potential of nucleic acid adducts can be readily determined through well-established mutagenicity assays such as the Ames test. Assays that identify the protein targets of electrophiles and other reactive exposure agents are necessary to identify their molecular mechanisms of toxicity.

One of the most popular herbicide classes over the past 50 years is the chloroacetanilides, which feature a highly electrophilic haloacetamide motif. These herbicides are N-alkoxy alkyl-N-chloroacetyl substituted derivatives of aniline and commonly used to minimize weed control for agricultural goods such as corn, maize, and rice[7]. Despite increased regulation due to evidence for carcinogenicity[8,9] and potential to accumulate in soil and wetlands[10], chloroacetanilides remain widely used throughout the world[11]. Although the reported carcinogenicity is presumably through the formation of DNA and protein adducts[12–14], other studies have found that

chloroacetanilides are not genotoxic and do not damage DNA *in vivo*[15]. Little work has been performed to identify which proteins are most susceptible to chloroacetanilide conjugation, and none at all to determine how this modification impacts protein stability (**Scheme 1A**).

Most of our knowledge regarding the protein targets of chloroacetanilides come from activity-based protein profiling (ABPP) experiments[16–18]. In these experiments, protein targets of a small molecule are identified based on their covalent reaction with a probe. Direct experiments substitute the small molecule with an isolable tag to generate the probe, while competition experiments use a probe with defined reactivity (e.g. for pK-pertubed cysteines) and profile proteins that can be competed out by the small molecule. Mice injected with acetochlor accumulated cysteine adducts in fatty acid oxidation pathway proteins with consequent metabolic deficits[16]. Broadly, most cysteines are not readily reactive to chloroacetamides, and even reactive cysteines show high specificity for individual ligands[18]. While powerful, this approach is limited to identifying proteins that form direct adducts with the probe. Pesticides and herbicides can produce secondary metabolites associated with protein damage and destabilization [19–21], leading to changes in protein stability[22–25], through mechanisms that should not change ABPP reactivity. More generally, loss of proteostasis for individual damaged proteins has the potential to destabilize the broader proteome[26–28].

Alternatively, a variety of proteome-wide methods assay changes in protein conformation or stability in response to exposure. These techniques, which include Stability of Proteins from Rates of Oxidation (SPROX), Fast Photochemical Oxidation of Proteins (FPOP), limited proteolysis (LiP), and Covalent Protein Painting (CPP), provide

residue-level interrogation of protein solvent accessibility[29–34]. Each has been successful at revealing ligand targets, and SPROX in particular has successfully identified targets of exogenous toxicants[35,36]. Still, these techniques require profiling of the entire proteome, which inherently challenges their depth.

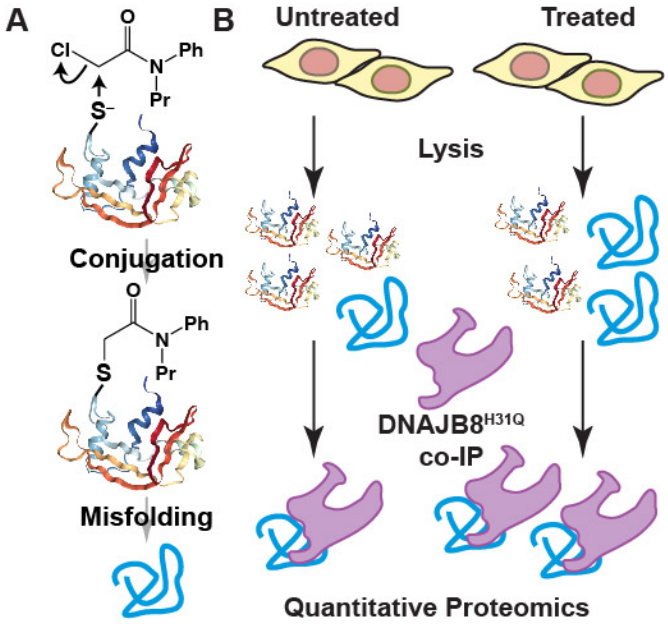

Scheme 1: A) Propachlor can conjugate to cysteine. This type of protein damage could induce protein misfolding. B) Description of our assay to identify changes in protein stability based on affinity to the Hsp40 DNAJB8^{H31Q}.

We previously developed an affinity purification mass spectrometry (AP-MS) approach to profile the misfolded proteome using human the Hsp40 DNAJB8 [37]. This assay combines affinity purification of overexpressed ^{Flag}DNAJB8^{H31Q} with quantitative proteomics to identify hundreds of co-isolating cellular proteins with high reproducibility and statistical confidence[38,39]. The H31Q mutation blocks the release of misfolded protein clients from DNAJB8, making it a thermodynamic sink for its clients. This binding is highly detergent-resistant, allowing immunoprecipitates to be stringently washed.

Proteins that are destabilized by a treatment are selected for by the affinity purification, and hence are more likely to be identified during LC-MS in data-dependent analysis mode.

Herein, we apply our Hps40 affinity platform to identify proteins that are destabilized after cellular exposure to chloroacetanilide herbicides. We profile the effects of acetochlor, alachlor, and propachlor on the HEK293T proteome and discovered distinct profiles of destabilized proteins for each condition, with most protein targets harboring reactive cysteines. Propachlor in particular targets Parksinsons' associated proteins GAPDH and PARK7, decreasing their cellular activity. Hsp40 affinity profiling is a simple method for rapidly identifying proteins that are destabilized by cellular exposure.

Materials and Methods

Materials: We purchased 1,4-dithiothreitol (DTT), Roche Protease Inhibitor cocktail w/o EDTA (PIC), HEPES, propachlor, acetochlor, alachlor, Tris (2-carboxyethyl)phosphine hydrochloride (TCEP), Sepharose-4B beads, M2 anti-Flag magnetic dynabeads, and the GAPDH Activity assay Kit from Sigma Aldrich. We purchased bovine serum albumin (BSA), Dulbecco's Modified Eagle Media (DMEM), Dulbecco's phosphate-buffered saline (DPBS), 10 cm tissue culture plates, and 6-well tissue culture plates from VWR. We purchased KCl, $MgCl_2$, $CaCl_2$, $Ag(NO_3)_2$, $Na_2S_2O_3$, NaCl, Tris-HCl, Triton X-100, sodium deoxycholate, urea, $Ca(O_2C_2H_3)_2$, glycerol, sodium dodecyl sulfate (SDS), poly D-lysine, and sequencing grade trypsin from Thermo Fisher Scientific. Proteinase K (PK) and Trypsin/LysC were purchased from Promega. Nanopure water was prepared

from a Millipore Milli-Q Laboratory Lab 4 Chassis Reagent Water System. 5 µm and 3 µm Aqua C18 resins were purchased from Phenomenex. 250 µm inner diameter fused silica columns were from Agilent. 100 µm inner diameter fused silica columns were from Polymicro. Strong cation exchange resin was from Partisphere, GE Healthcare. Rapigest was purchased from Aobious (Gloucester, MA). TMT-6plex isotopic labels were from Pierce. Bradford reagent was purchased from Bio-rad. Ambient temperature in our laboratory is maintained between 17 and 21 °C.

Cell Culture and Immunoblotting: HEK293T cells were maintained in DMEM supplemented with glutamine, penicillin, streptomycin, and fetal bovine serum (Seradigm). ^{Flag}DNAJB8^{H31Q} plasmid has been reported previously[38]. ^{Flag}GAPDH in the pCMV3 vector was purchased from Sino Biological. Immunoblots were transferred to nitrocellulose from SDS-PAGE gels using a Bio-Rad Trans-Blot Turbo, stained with ponceau S to image total protein, blocked with 5% dried milk/TBST (10 mM Tris pH 7.4, 150 mM NaCl, 0.1% Tween), washed with TBST, incubated with primary antibody in 5% BSA/TBS with 0.1% NaN_3, washed with TBST, incubated with near-IR conjugated secondary antibody in 5% dried milk/TBST, washed with TBST, washed with TBS, and imaged on a Li-COR Fc.

AP-TMT-MudPIT: TMT-AP-MS experiments using ^{Flag}DNAJB8^{H31Q} were performed as described previously[37]. Briefly, six 10 cm plates of HEK293T cells were transfected by the calcium phosphate method with 5 µg of plasmid DNA encoding ^{Flag}DNAJB8^{H31Q} in the pFLAG backbone. Plates were treated with 1 mM of the indicated chloroacetanilide

at 40-46 hours post transfection for 30 min in serum free media. Cells were harvested by scraping in DPBS. Cells were then lysed in 9 parts RIPA Buffer (150 mM NaCl, 50 mM Tris pH 7.5, 1% Triton X-100, 0.5% sodium deoxycholate, 0.1% SDS) and 1 part 10x PIC on ice for 30 min. Samples were centrifuged 21,000 x g for 15 min at 4 °C to separate lysate from cell debris. The Bradford assay was used to quantify protein in each lysate. Lysates were incubated with 15 µL Sepharose-4B beads for 30 min at 4 °C, then centrifuged at 1,500 x g for 1 min to pellet beads. Lysate was then separated and then incubated with 15 µL of M2 anti-Flag Magnetic Beads and rotated overnight at 4 °C. The anti-Flag beads were washed the next day four times with RIPA buffer. Each wash included rotation for 10 minutes at ambient temperature. Proteins bound to the anti-Flag beads were eluted by boiling for 5 min at 100 °C in 30 µL of Laemmli concentrate (120 mM Tris pH 6.8, 60% glycerol, 12% SDS, brilliant phenol blue to color). 5 µL of the elutes were saved for silver stain analysis and the remainder was prepped for mass spectrometry and TMT-labeled from a 6-plex TMT set.

Only MS quality organic solvents were used during sample preparation. Samples were $CHCl_3$/MeOH precipitated, resuspended in 1% Rapigest, diluted in 50 mM HEPES pH 8.0, reducing 30 min. with 5 mM TCEP, alkylated for 30 min in the dark with 10 mM iodoacetamide, digested with 500 ng trypsin overnight at 600 rpm and 27 °C, labeled with the appropriate TMT tag NHS-ester in 40% acetonitrile for 1 h, quenched with ammonium bicarbonate, pooled, acidified by being brought to 5% formic acid, and clarified by centrifugation for 30 min. at 21000 *x g*. The composition for buffer A is 0.1% formic acid, 5% acetonitrile in water. The composition for Buffer B is 0.1% formic acid,

80% acetonitrile in water. The composition for Buffer C is 500 mM ammonium acetate in Buffer A. MS runs were performed by using a two-dimensional LC/MS/MS setup on an LTQ Orbitrap Velos Pro hybrid mass spectrometer (Thermo) interfaced with an Easy-nLC 1000 (Thermo) according to standard MuDPIT protocols[40]. For each run, MS/MS spectra were extracted using MSConvert (version 3.0.21144) with Peak Picking Filtering. FragPipe was used to search MS/MS spectra against a Uniprot human proteome database (06/11/2021 release, longest entry for each protein) supplemented with common contaminants and reverse sequence decoys for a total of 40858 sequences[41]. MS/MS spectra were also searched against 20429 select decoys (e.g albumen, porcine trypsin, contaminants etc.). FragPipe searches allowed for static modification of cysteine residues (57.02146 Da, acetylation), variable modifications of herbicide adducts (175.0997 for propachlor adducts, 233.1416 for acetochlor and alachlor adducts), static TMT taggin of N-termini and lysine residues (229.1629 Da), and half tryptic peptidolysis specificity. We allowed a mass tolerance of 1.25 Da for the precursor ion mass and 20 ppm for the product ion masses. MSFragger (Version 3.2) was used to match and filter spectra. Decoy proteins, common contaminants, immunoglobulins, and keratins were filtered from the final protein list. Quantitation in FragPipe was performed by averaging TMT reporter ion intensities for all spectra associated with an individual peptide. Raw proteomics data is available through the PRIDE Archive at PXD030635.

^{Flag}GAPDH AP-MS was performed similarly, except digestion was performed using two step LysC/Trypsin (Promega) digestion according to manufacturer's protocol, and

dynamic exclusion was set to 30 seconds during LC-MS/MS analysis of peptides. Open search was performed in FragPipe using default settings[42]. For intact protein MS, beads were washed 4 times with PBS after RIPA washes and eluted overnight in 8.8 M urea in 50 mM Tris pH 8.0. Quantitative immunodepletion was confirmed by immunoblotting, sample purity was confirmed by SDS-PAGE followed by silver stain, and samples were analyzed by LC-ESI-MS on an Agilent 6545 LC/QTOF. Charge state envelopes were deconvoluted using MassHunter Bioconfirm software.

Statistical Analysis: Statistical analysis was performed as previously described[37]. Initially, protein-level intensities were normalized to the intensity of bait (DNAJB8) in each TMT channel. We then used a version of the scaled reference approach to combine multiple TMT runs[43]. The bait-normalized integrated TMT reporter ion intensities were averaged for each protein across the three control conditions in each AP-MS run to get a scaling factor. Each bait-normalized protein intensity was then divided by this scaling factor. Storey's modification of the method of Benjamini and Hochberg was used to convert unadjusted p-values to q-values (local false discovery rates)[44,45]. Unadjusted p-values were ranked in increasing order and the q-value for the *i*th protein determined from:

$$q_i = \pi \, min_{i \le j \le n} \frac{pn}{i}$$

Storey's modification is performed by determining the overrepresentation of low p-values to infer a global false discovery rate, and then scaling local false discovery rates accordingly. The π-factor for this scaling was 0.54 for the acetochlor treatment, 0.5 for alachlor treatment, and 0.3 for propachlor treatment.

Limited Proteolysis and PRM: The limited proteolysis procedure was optimized from standard protocols and previous experiments[33,37]. 1 mg/ml stocks were prepared from 25 mg of lyophilized Proteinase K (PK) were dissolved in storage buffer (50 mM Tris-HCl, 2 mM calcium acetate, pH 8.0) and stored at –70 °C. The following concentrations of PK were prepared from serial dilutions from the 1 mg/ml aliquot: 0.5 mg/ml, 0.2 mg/ml, 0.1 mg/ml, 0.05 mg/ml, and added to lysate to yield 1:200, 1:500, 1:1000, and 1:2000 protease:substrate protein ratios (w/w) respectively. 2 µl PK was added to a 200-µg aliquot of protein lysate and incubated for 1 min at 25.0 °C for each digestion. Samples were then boiled for 5 min to quench PK activity. Three separate digestions were performed for the no PK condition for each lysate sample. Samples were prepared for mass spectrometry were analyzed using LC-MS/MS and parallel reaction monitoring (PRM). Chromatograms and product ions were quantified by Skyline[46].

PRM runs were performed using the following gradient of Buffer A to Buffer B. The composition of Buffer is 5% acetonitrile and 0.1% formic acid in Millipore water. Buffer B is composed of 80% acetonitrile and 0.1% formic acid in water. Peptide were separated by LC-MS using a 100 minute gradient composed of Buffer A (5% acetonitrile:95 % water: 0.1% formic acid) and Buffer B (80% acetonitrile: 20% water: 0.1% formic acid) over the following segments: 1-5 min: 1-6% Buffer B. 5-75 min: 6-33% Buffer B. 75-80 min: 33-100% Buffer B. 80-85 min: 100% Buffer B. 85-90 min: 100-1% Buffer B. 90-100 min: 1% Buffer B. Flow rate was 500 nl/min. Technical and biological CVs for each peptide were below 20%, except for VPTANVSVVDLTCR which exhibited a CV of 22%

between runs (**Table S1**). CVs of select peptides were analyzed at 60000 resolving power for MS2 scans using unscheduled runs and were not meaningfully affected, confirming that 7500 is adequate to avoid interference (**Table S1**).

GAPDH Activity Assay: GAPDH enzymatic activity in cell lysates were measured using an assay kit (Sigma MAK277) according to the manufacturer's protocol. Three 10 cm plates of HEK293T cells were treated with 1 mM propachlor for 30 minutes in serum-free media and three 10 cm plates of HEK293T cells were treated with DMSO in serum free media for 30 minutes. Each plate was then harvested by scraping with DPBS and pellets were frozen in -80 ^{o}C for future use. Each pellet was lysed in GAPDH Assay buffer and 8 µL from each plate were aliquoted into a separate row for 4 wells where each well had 42 µL of GAPDH assay buffer including GAPDH Developer. There were 6 rows used in the plate. 2 wells were treated with GAPDH substrate, and 2 wells were treated without substrate. Measurements were recorded on a Bio-tek Synergy H1 microplate reader. Absorbance measurements were recorded at 450 nm and normalized to protein concentration measured by Bradford.

DJ-1 Deglycase Activity Assay: DJ-1 (PARK7) Deglycase Assay was modified from Tsumoto et al.[47] 6–cm plates of HEK293T cells were grown to 80% confluency, followed by pre-treatment with either 1 mM propachlor or vehicle (DMSO) for 30 min in serum-free media. They media was then changed to complete media with or without glyoxal for 2 h, followed by immediate harvest by scraping with DPBS and lysis in 9 parts RIPA Buffer (150 mM NaCl, 50 mM Tris pH 7.5, 1% Triton X-100, 0.5% sodium deoxycholate,

0.1% SDS) and 1 part 10x PIC for 30 min on ice. Cell lysates were quantified by Bradford and loaded on 10% SDS page gels for western blotting analysis. Western blots were first probed with anti-carboxymethyllysine antibody (CML; rabbit polyclonal) and then with anti-β-actin (mouse monoclonal 7D2C10).

Propachlor Aggregation Studies: Three out of six 10 cm plates of HEK293T cells were treated with 1 mM propachlor for 30 min. The other three 10 cm plates were treated with DMSO for 30 min. Media was then changed for recovery for 6 h. Cells were harvested by scraping in DPBS and lysed in 9 parts RIPA Buffer (150 mM NaCl, 50 mM Tris pH 7.5, 1% Triton X-100, 0.5% sodium deoxycholate, 0.1% SDS) and 1 part 10x PIC for 30 min on ice. Lysate was separated from cell debris by centrifugation at 21,000 x g for 15 minutes at 4 °C. Protein in the lysate was quantified by Bradford. Protein samples were normalized and balanced to 2mg in 1ml of RIPA. The rest left is a representative of total (T) sample. Samples were placed in TLA-SS rotor and spun in a Beckman Opti-MAX at 77,000g for four hours. Soluble fraction was separated from insoluble fraction. The insoluble fraction was washed four times with RIPA buffer. Each wash included gentle resuspension for 1 minute. The insoluble fraction (P) was resolubilized in 8 M urea in 50 mM Tris overnight at 4 ^{o}C. Aliquots from initial lysis, soluble fraction, and insoluble fraction was taken for western blot analysis.

Two separate TMT experiments were used to quantify changes in aggregation between propachlor and control treated samples. TMT sample prep was adapted from labeling procedure from AP-TMT-MuDPIT experiments. Only MS quality organic solvents were

used during sample preparation. Aliquots of 20 µg were taken from each T sample. Samples were precipitated by methanol/chloroform precipitation. Pellets were then air-dried and resuspended in 1% rapigest in water. Resuspended protein solutions were then diluted to 50 µL in 100 mM HEPES, pH 8.0, and reduced with 10 mM TCEP for 30 min at 37 °C. Protein solutions were then alkylated with 5 mM iodoacetamide for 30 min in the dark at ambient temperature. 0.5 µg sequencing grade trypsin was added to the protein solution for digestion overnight at 37 °C with agitation (600 rpm). TMT isotopic labels were resuspended (100 ug/80 µL acetonitrile) and 40 µL of label was added to each 60 µL sample of digested peptides. Samples were labeled for 1 h at ambient temperature. Labeling was quenched with 0.4% ammonium bicarbonate at ambient temperature for 1 h. Samples were pooled, acidified, centrifuged for 30 min at 21,100 x g to remove any insoluble debris. Samples were then dried by centrifugal evaporation to 10 µL. Solutions were then brought to 200 µL in Buffer A, incubated at 37 °C for 1 h, and centrifuged for 30 minutes at 21,100 x g. Solutions were transferred to new low-binding tubes (Eppendorf) and the process of heat-spinning was repeated three more times to complete elimination of Rapigest.

Pellet (P) fractions were quantified by Bradford. The amount of sample required to make 20 µg of protein was averaged among the 6 samples. That average aliquot was then taken from each sample and precipitated by methanol/chloroform precipitation. The sample was then labeled as shown above for the T fractions.

Resazurin Assay: Resazurin sodium salt was purchased from Acros Organic. For cell viability experiments exploring propachlor treatments, 50,000 cells were plated in 64 wells in a Poly-D-Lysine coated 96 well plate. Each row was treated with an increasing amount of propachlor for 30 minutes starting with 0 mM to 1 mM propachlor in serum free media. The media was then changed and allowed to recover for 24 hours. Two mg of resazurin sodium salt was resuspended in 1 ml of DPBS. 5 µl of resazurin solution was added to each well. The final concentration for each well was thus 380 µM. Fluorescence measurements were recorded on a Bio-tek Synergy H1 microplate reader at 550 nm excitation and 590 nm emission. The bandwith filter selected for excitation was from 540-560 nm. The bandwith filter for emission was from 580-600 nm.

Results and Discussion

Because our assay uses recovery of proteins with DNAJB8^{H31Q} as a proxy for affinity, changes in protein abundance would complicate the interpretation. To avoid perturbation to proteome abundance, we optimized the treatment time to be short enough to preclude transcriptional and translational remodeling of the cell[37,48] while still inducing protein destabilization. The primary misfolded protein stress response in the cell is the Heat Shock Response (HSR), in which the presence of nuclear or cytosolic misfolded proteins activates the transcription factor HSF1, leading to increased transcription and translation of chaperones and degradation factors and consequent restoration of cellular protein homeostasis[49]. A primary chaperone target of HSF1 is the cytosolic Hsp70 HSPA1A. We validated that 30 min 1 mM of acetochlor in serum-free media followed by a 16 h recovery, induces HSR target HSPA1A in HEK293T cells in cells overexpressing ^{Flag}DNAJB8^{H31Q} (**Figure 1**). Treatment with 1 mM acetochlor for 30 minutes in serum-free media was thus chosen for profiling using our AP-MS strategy. Serum-free media is necessary to avoid small molecule scavenging and is a standard incubation condition for cellular exposure to acetochlor[16,50,51]. Indeed, the use of complete media ablates HSR activation by acetochlor. Surprisingly, ^{Flag}DNAJB8^{H31Q} sensitizes the cells to activate the HSR in response to acetochlor treatment, possibly due to its direct binding of misfolded client proteins[52–54]. This sensitization was not previously observed for HSR induction by arsenite or by cadmium[37]. 1 mM propachlor and 1 mM alachlor in serum-free media for 30 minutes were chosen to be consistent with the acetochlor conditions despite neither herbicide upregulating HSPA1A (**Figure S1A,B)**. Using the same conditions for each herbicide treatment allows us to relate

effects on the proteome to structural characteristics rather than to incubation time and concentration. Even in the absence of adequate global proteostatic stress for HSF1 activation, propachlor and alachlor could still induce misfolding of specific protein targets with consequent cellular toxicity[55]. Consistent with this possibility, we found that 30 min. incubation with 1 mM propachlor inhibits viability of HEK293T cells by resazurin assay (**Figure S2**).

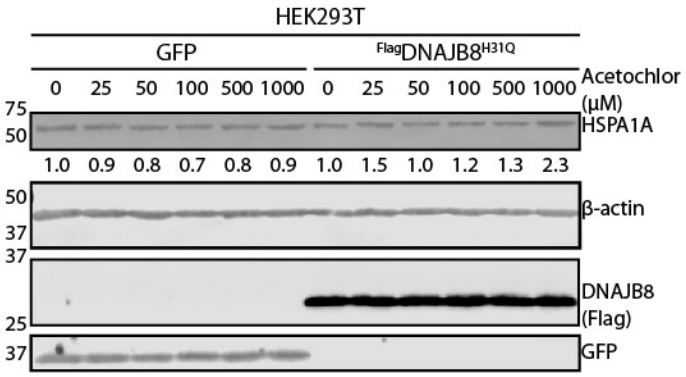

Figure 1: Immunoblot of SDS-PAGE separated lysates from HEK293T cells expressing the indicated proteins and treated with acetochlor in serum-free media for 30 min., followed by a 16 h recovery in complete media. Induction of the HSR target HSPA1A in response to acetochlor treatment is a proxy for the level of HSR activation. HSPA1A density is below the blot slice. Molecular weight markers are indicated on the left. Antigens targeted by immunoblotting are listed to the right of the slice.

We utilized the Hsp40 affinity approach **(Scheme 1)** to profile for chloroacetanilide-dependent misfolded proteomes. ^{Flag}DNAJB8^{H31Q} was transiently overexpressed in HEK293T cells, followed by 30 min of chloroacetanilide herbicide treatment, and immediate Flag immunoprecipitation from cellular lysate. Co-immunoprecipitated proteins were labeled by TMT isobaric tagging[56] and then identified and quantified by LC/LC-MS/MS. Each herbicide treatment (acetochlor, alachlor, and propachlor) was performed over 24 biological replicates (12 treated and 12 controls) and analyzed by four 6-plex TMT runs. The overall protein distribution in eluates, as analyzed by SDS-

PAGE separation followed by silver staining, does not show gross differences between the immunoprecipitates, as expected from such a short treatment (**Figure S3**).

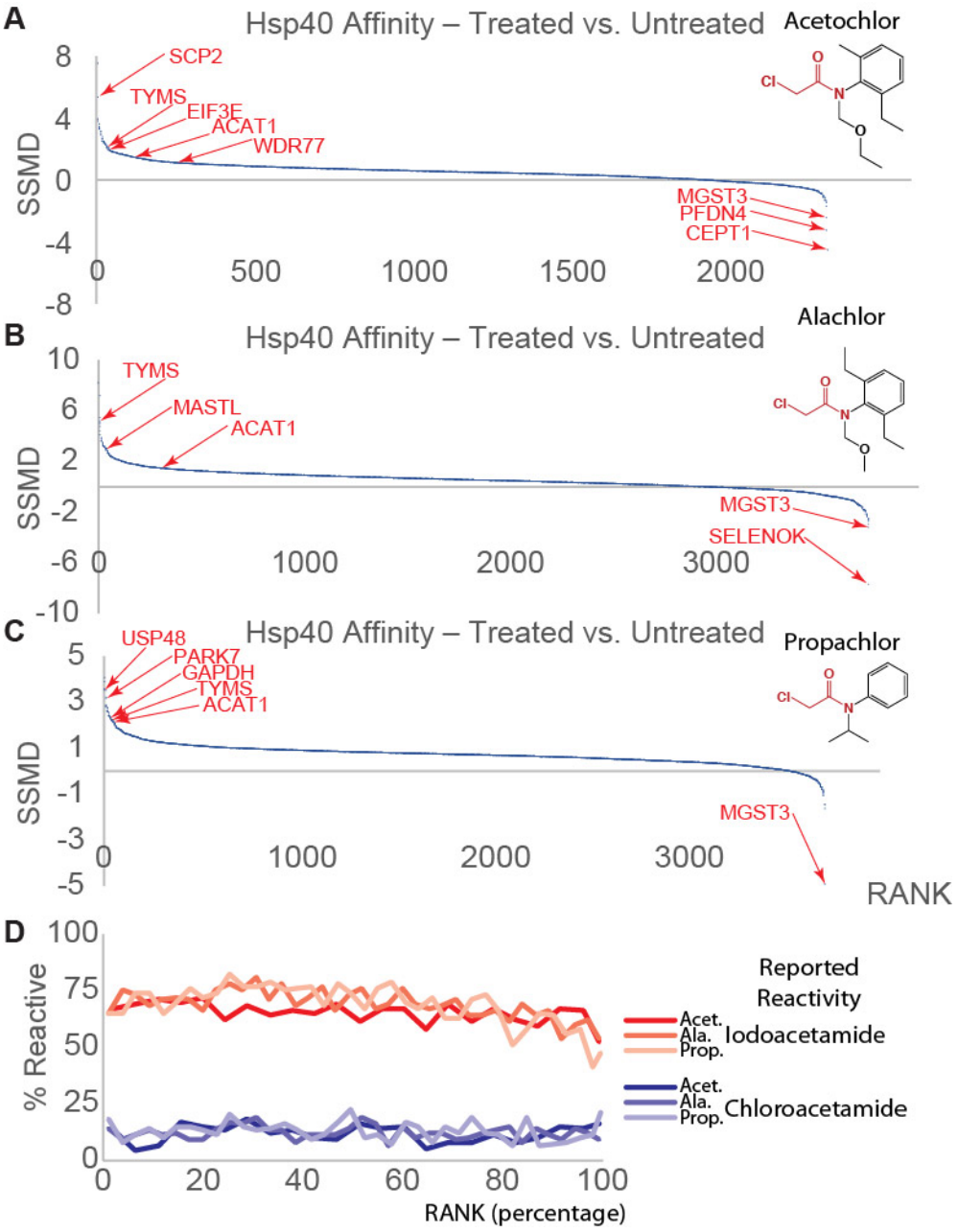

Figure 2: **A-C.** Differential Hsp40 affinity of proteins in response to treatment (1 mM, 30 min. in serum-free media, n = 4 biological replicates) of HEK293T cells with the indicated herbicides. The DNAJB8^{H31Q}-interacting proteins are ranked by Strictly Standardized Mean Differences (SSMDs, variance-normalized differences between control and treatment). Notable proteins are indicated by red arrows. **D.** Percent of proteins (binned in groups of 100 according to ranked SSMD) that were reported as

reactive to a general iodoacetamide probe or any of 128 chloroacetamide probes in Kuljanin et al.[18]. Volcano plots can be found in **Figures S3-5**.

The Hsp40 affinity profile for each chloroacetanilide exposure provides a distinct fingerprint (**Tables S2-S4**). Acetochlor treatment increases DNAJB8 affinity for most (82%) of DNAJB8 clients identified across the mass spectrometry runs (**See Figure 2A** and **Figure S4)**, with 2% of clients demonstrating a greater than 2 fold increase in affinity. We further compared to a previously reported liver ABPP of mice exposed to acetochlor[16]. Out of 338 common quantified proteins, there is no correlation (**Figure S5**, $R^2 < 0.01$) between the extent to which proteins are destabilized according to the Hsp40 assay and the extent to which they lose iodoacetamide reactivity following acetochlor exposure, indicating that our assay is distinct from measuring conjugation. Of the 28 mouse liver proteins that lost iodoacetamide reactivity **or** alkynylated acetochlor reactivity following mouse acetochlor treatment, 20 were identified in our Hsp40 affinity runs, with 6 demonstrating significantly (q-value < 0.05) increased Hsp40 affinity (SCP2, ACAT1, PDIA3, NNT, HSPD1, and DLD). Given the differences in model system (intraperitoneal injection of mice followed by *ex vivo* liver excision and alkynylated iodoacetamide labeling vs. human tissue culture) and in the assays, it is encouraging that several of the same targets are found in both studies.

Several enzymes with active cysteines prone to electrophilic modification had significantly greater affinity for $DNAJB8^{H31Q}$ after acetochlor exposure. Thymidylate Synthase (TYMS) (Fold Change = 3, q value = .003), an enzyme essential for production of thymidine nucleotides[57], has an active site cysteine that is specifically targeted by an electrophilic chemotherapeutic drug[58]. Another protein with significantly

increased Hsp40 affinity following acetochlor treatment is eukaryotic translation initiation factor 3 subunit E (eIF3e) (Fold Change = 1.96, q value = .0004) which plays a role in tumor growth and the hypoxia response[59]. Acetyl-CoA acetyltransferase 1 (ACAT1; Fold change = 2.91, q value = .02) was significantly destabilized, consistent with its multiple reactive cysteines[18,60,61]. It's possible that adduct formation could stabilize rather than destabilize a protein, leading to a decrease in Hsp40 affinity. Choline /ethanolaminephosphotransferase 1 (CEPT1) and microsomal glutathionine S-transferase 3 (MGST3) bind less to DNAJB8^{H31Q} after treatment, indicating stabilization. These two enzymes both contain active site cysteines that interact with substrates (ethanolamine phosphate and glutathione respectively)[62,63]. Alternatively, these proteins could have lower abundance in response to propachlor treatment, though CEPT1 and MGST3 are both fairly long-lived proteins[64,65] and so would have to be actively degraded to be depleted on the time-scale of the experiment.

Despite its lack of HSR induction, alachlor exposure increases DNAJB8 affinity of many more proteins than acetochlor exposure (**Figure 2B** and **Figure S6)**. 764 proteins show significantly (q-value < 0.05) increased DNAJB8 affinity following alachlor exposure, as opposed to 81 proteins following acetochlor exposure. Selectively targeted proteins included Microtubule Associated Serine/Threonine Kinase Like (MASTL) (fold change = 2.02, q value = 5 x 10^{-5}), a kinase involved in mitosis[66], and Zinc Finger Protein 24 (ZNF24), a tumor suppressor[67]. The higher impact of alachlor as opposed to acetachlor is in some ways surprising, as the two molecules are isomers differing only by a methyl group. However, regioisomers can have substantially different lipophilicities and cellular uptake[68]. Alachlor has a log K_{ow} of 3.5, as opposed to 3.0 for acetachlor.

Small structural differences have been shown to have large effects on protein reactivity for other electrophilic series[69]. The stronger protein destabilization response to alachlor treatment could also reflect the differential metabolism of the compounds. Compared to alachlor, acetochlor metabolizes faster into 2-chloro-N-(2,6-diethylphenyl)acetamide (CMEPA) and 2-methyl-6-ethylaniline (MEA)[70,71]. While microsomal pathways are not available in the HEK293T cells, other chloroacetanilide decomposition pathways could be available.

Propachlor treatment has the strongest effect on the DNAJB8^{H31Q}-associated proteome (**Figure 2C** and **Figure S7**). The two most prominent targets that are unique to propachlor are glyceraldehyde-3-phosphate dehydrogenase (GAPDH; fold change = 5.97, q-value = 6.09 x10^{-5}) and Parkinson's disease protein 7 (PARK7/DJ-1, fold change = 3.8, q-value = 5.56 x 10^{-6}). GAPDH is an enzyme that canonically uses a susceptible active-site cysteine to bind and reduce nicotinamide adenine dinucleotide (NAD) in glycolysis[72], but consistent with its high abundance also engages in extensive moonlighting activities[73]. Due to its high abundance and pK-perturbed active site cysteines, GAPDH is a frequent conjugation target of electrophilic molecules[74,75]. GAPDH is found in Parkinson's Disease (PD)-associated aggregates, and its aggregation is promoted by electrophilic conjugation[76]. Given its abundance and fold change in DNAJB8 co-IP recovery, it is possible that GAPDH is the feature observed by silver stain at 37 kDa (**Figure S3**). Thermodynamically destabilized PARK7 variants are linked to familial Parkinson's disease[77], and PARK7 overexpression protects against chemical induction of Parkinson's phenotypes[78]. Although a wide variety of mechanisms have been ascribed to PARK7, including chaperoning and proteolytic activities, the evidence is strong that it serves as an oxidative stress sensor that protects against

cysteine oxidation[79], as well as a cellular deglycase preventing electrophilic protein damage.

We expected that proteins with the highest reactivities to electrophilic species would also be the most destabilized, while proteins whose Hps40 affinities are less impacted by propachlor treatment would be enriched in less reactive proteins. We compared the ranked SSMDs for all identified proteins against reactivity profiles reported in Kuljanin et al.[18], with the expectation that our strongest hits for each chloroacetanilide would reflect proteins that are generally more active nucleophiles. Proteins were considered to be iodoacetamide-reactive if they were directly modified by the iodoacetamide probe, and were considered chloroacetamide-reactive if any of the 158 tested chloroacetamides could outcompete iodoacetamide reactivity by a factor of 4-fold (**Figure 2D**). For each chloroacetanilide herbicide, there is no enrichment of more reported reactive proteins at higher Hsp40 affinity follow herbicide treatment. About 12% of our identified proteins have reported chloroacetamide reactivity, independent of chloroacetanilide-induced destabilization. This finding strongly agrees with a central conclusion from the prior work: chloroacetamide reactivity is sparse, with most molecules showing substantial specificity to individual proteins. In keeping with the greater reactivity of iodoacetamides, about 70% of our identified proteins have reported iodoacetamide reactivity, again independent of chloroacetanilide-induced destabilization. This finding is more surprising, but could reflect that Hsp40 affinity is not the same as reactivity; adduct formation can have different effects on protein stability for different proteins. Indeed, there is no correlation between the promiscuity of a protein for chloroacetamide modification and it's destabilization by any of the three

chloroacetanilides that we profiled (**Figure S8**). Nevertheless, our most affected proteins are iodoacetamide reactive, consistent with the primary mechanism of protein destabilization due to cellular chloroacetanilide exposure being mediated through direct conjugation at reactive cysteines (**Figure S9**).

Including PARK7 and GAPDH, 78 proteins have substantially increased (fold change > 2 and q-value < 0.1) affinity for DNAJB8 following propachlor treatment (**Figure 3A**). This is more than the twice the combined number of proteins destabilized under the same criteria after alachlor and acetochlor treatments. The higher susceptibility of the proteome to propachlor could be based on substitution reaction reactivity. Kinetic studies between propachlor and alachlor reactivity found a 2-fold increase in the substitution of propachlor against several nucleophiles and a lower Gibbs free energy required for substitution reactions of propachlor with nucleophilic thiols[80]. All three treatments cause marked destabilization of TYMS and ACAT1, and apparent stabilization (decreased DNAJB8 affinity) of CEPT1 and MGST3 (**Figure 3B**). Outside of those, the proteins that are most affected by each individual treatment are unique. This selectivity is particularly salient given the high concentrations (1 mM) used for the treatments. The unique profiles of proteins affected by each herbicide is consistent with the high selectivity of protein reactivity with even strongly reactive warheads [81–83].

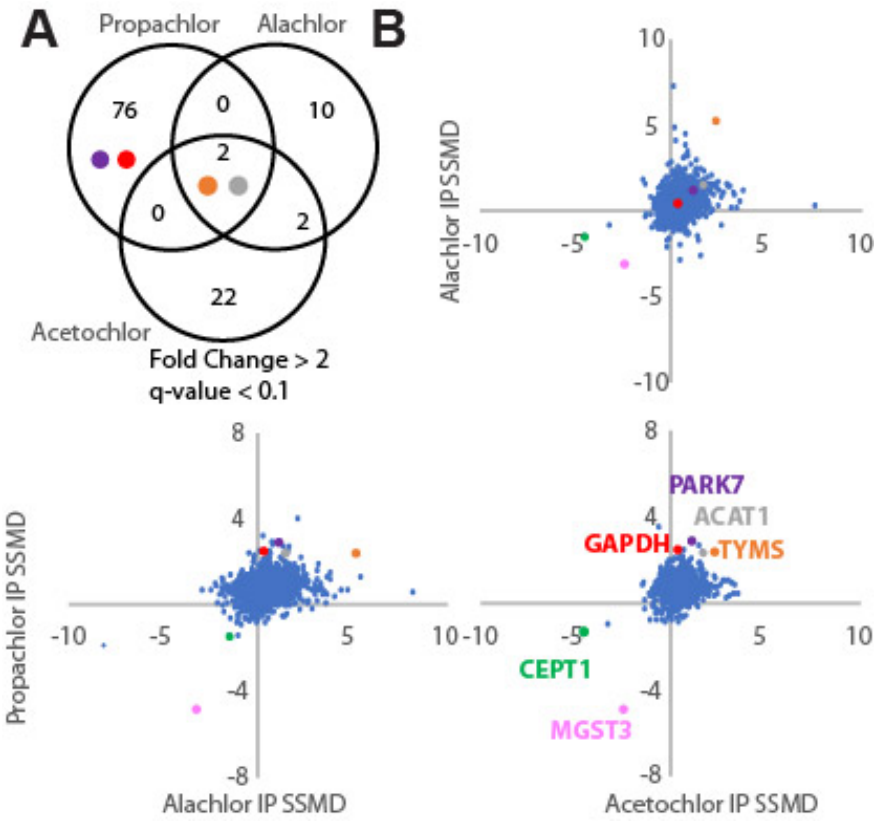

Figure 3: Comparison of proteome-wide Hsp40 affinity changes from the three chloroacetanilide herbicide treatments. **A.** Comparison of the most impacted proteins and **B.** Comparison of Strictly Standardized Mean Differences (SSMDs; treatment vs. control). Coloring of points in this figure is used consistently to show relative reactivities of PARK7, ACAT1, TYMS, GAPDH, CEPT1, and MGST3.

We searched for cysteine-chloroacetanilide adducts from each run, finding 32/8637, 40/16029, and 102/15694 modified/total peptides following acetochlor, alachlor, and propachlor treatments respectively. It can be challenging to identify peptide modifications without enriching for the modified sites, as stoichiometry on a per peptide basis for post-translational modifications are often low[84]. Furthermore, when peptide identifications are filtered, the filtration thresholds are set for each search such that the false discovery rate based on a decoy set is <1% of peptides. While that intended threshold is likely reasonably close to the true false discovery rate in the

context of the entire proteome[85], for a modification found on only a small number of modified peptides it introduces a much higher practical risk of misidentification[86]. With these caveats in mind, we include the list of identified chloroacetanilide conjugates in **Table S5**. It is also worth noting that we consistently see a DNAJB8 modification at C70. While this is in the DNAJB8 J-domain[53,87], which is dispensable for client binding, we cannot rule out the possibility that this modification itself could impact DNAJB8 recognition.

Protein misfolding is a necessary intermediate step for protein aggregation[88,89] and all misfolded proteins have the potential to aggregate[90]. The increase in protein misfolding following propachlor exposure could also lead to an increase in aggregation. We used ultracentrifugation to isolate the insoluble proteome following cellular propachlor exposure (**Figure 4** and **Table S6**). Cells were allowed to recover 6 h post-treatment to allow misfolded proteins time to partition towards an aggregated state. Nearly all detected proteins aggregate more in response to cellular propachlor exposure (**Figure 4** and **Figure S10**). Propachlor treatment has no significant effect on lysate protein abundances, suggesting that the cellular proteome is not meaningfully remodeled over this time-scale (**Figure S11**).

Despite both aggregation and Hsp40 affinity increasing across a majority of the observed proteome after cellular propachlor exposure, there is no meaningful correlation between these two factors. This is consistent with a previous study that found that stress-dependent protein aggregation does not correlate with stability across diverse stresses[91]. Generally, different measures of protein stabilization are poorly correlated with each other, as protein misfolding involves multiple processes that will be

probed differently by different assays[34]. The vesicular trafficking proteins[92,93] SMAP2, GAK, CLTA, CLTB, CLTC, CLTC1, AP1B1, AP1M1, EPS15, and CLINT1 all substantially lose solubility in response to propachlor treatment, but this network only modestly increases its DNAJB8 affinity. These proteins rely on Hsp70 for clathrin disaggregation, but GAK serves as a dedicated Hsp40 co-chaperone outside of neuronal cells[27,94]. These proteins may not be well-surveyed by a promiscuous Hsp40 such as DNAJB8, even under conditions that lead to their destabilization. Alternatively, they may have lower thresholds for aggregation as compared to proteins that show greater differential DNAJB8 affinity following propachlor treatment[95].

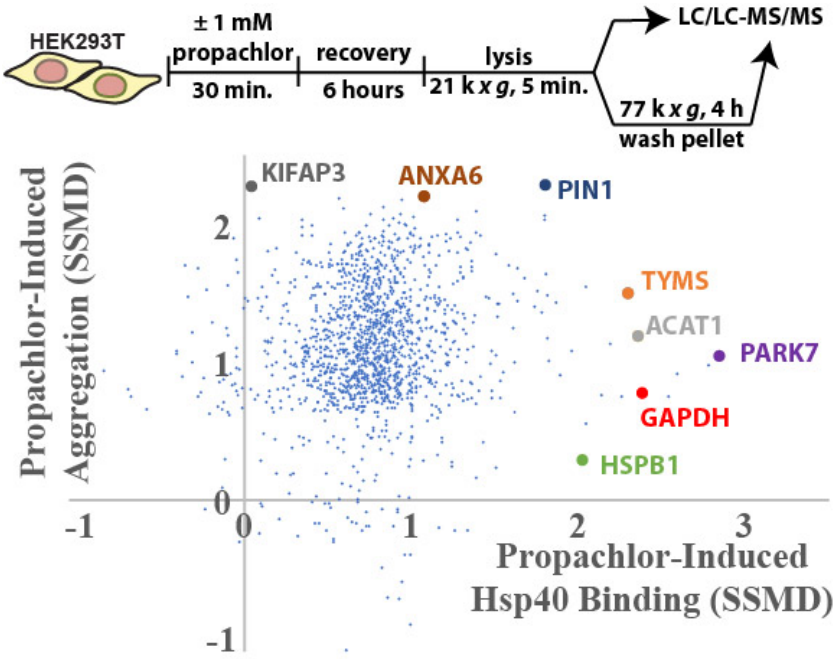

Figure 4: Aggregation of cellular proteins in response to propachlor exposure. Strictly standardized mean deviations (SSMDs) for propachlor-dependent protein insolubility and Hsp40 affinity. HEK293T cells were treated as indicated, lysed, pre-clarified by centrifugation, and the lysates normalized to total protein. Protein aggregates were further prepared by ultracentrifugation (6 biological replicates for each treatment condition). The plot compares the change in aggregate levels for each protein to the change in Hsp40 binding (from **Figure 2C**) for proteins identified in both sets of experiments (1477 proteins). Volcano plots for both propachlor-dependent changes in the total and aggregated proteome are in **Figures S10 and S11**.

GAPDH is highly abundant in the human proteome with many functions beyond its canonical role in glycolysis[72,73]. These functions are readily perturbed by a diverse range of post-translational modifications[96] which can lead to toxic aggregation[97], making its destabilization following propachlor exposure particularly hazardous for cellular proteostasis. Hence, we looked for the presence of GAPDH-propachlor adducts. GAPDH is susceptible to modification by a wide range of electrophiles, including 4-hydroxynonenal and methylglyoxal[98,99]. Cysteines in the NAD+ binding site are particularly subject to electrophilic modification[100–102]. To determine whether GAPDH is modified during propachlor treatment, we immunoprecipitated ^{Flag}GAPDH from lysates following cellular propachlor treatment. GAPDH interactions are interrupted by our stringent RIPA washes, so that ^{Flag}GAPDH is prepared with minimal contamination by other proteins (**Figure S12A**). In the absence of treatment, we see GAPDH primarily present as the N-terminally acetylated protein, with a smaller population of the glutathione conjugate (**Figure S12B**). After propachlor treatment, we see a new base peak at +176 Da, consistent with a single propachlor adduct (**Figure S12C**). No evidence of multiple adducts is observed. We further investigated immunoprecipitated ^{Flag}GAPDH by digestion and shotgun proteomics, followed by an open adduct search[42]. The propachlor modification is clearly localized to C152 based on MS2 spectra (46 total spectral counts) (**Figure 5**). C152 is in the NAD^+ binding site, and is necessary for catalytic activity[103]. Across two biological duplicates, we find a 26±7% drop in the unmodified C152 intensity, implying that about a quarter of GAPDH is modified. No evidence for modification at C156 was observed.

To understand how global stability of GAPDH is impacted by propachlor treatment, we profiled the rest of the protein using targeted limited proteolysis[37]. Destabilized protein domains are more extended and thus more susceptible to cleavage by a promiscuous protease, such as thermolysin or proteinase K (PK)[104]. LiP involves brief treatment of lysate to protease followed by shotgun proteomics to characterize the yield of cleavage events[31,105,106]. Loss of a tryptic peptide indicates a protein conformational change in the vicinity of that peptide sequence[107].

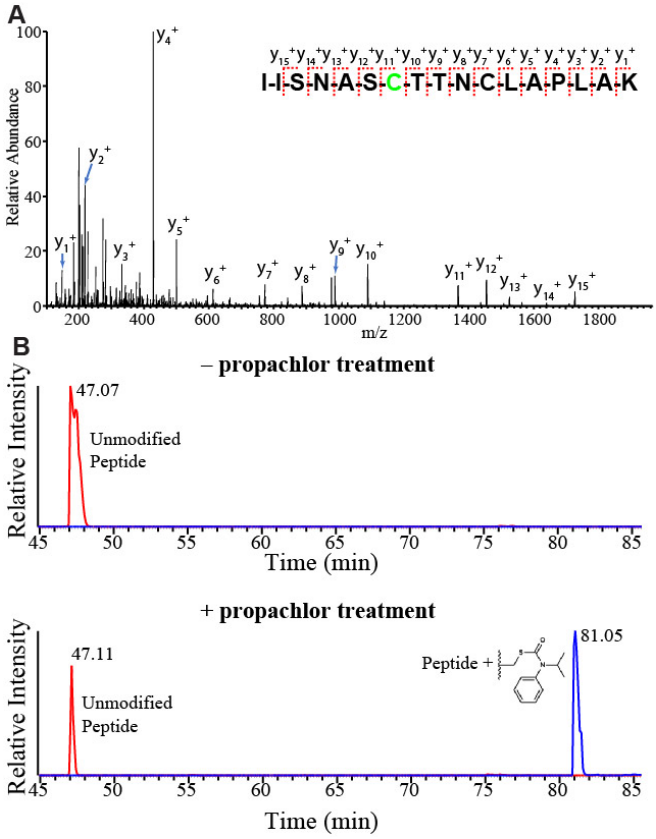

Figure 5: Propachlor modifies a catalytic cysteine in the active site. A) MS2 fragmentation spectrum obtained from LC-MS/MS shotgun proteomics analysis of lysate collected from propachlor treated (1 mM, 30 min., serum-free media) HEK293T cells. This peptide is modified at the C152 position with an adduct that corresponds to propachlor thiocarbamate. C156 is carbamidoylated by iodoacetamide. B) PRM chromatograms demonstrating the dependence of the adduct on propachlor treatment.

We selected peptides from GAPDH for LiP to assess structural changes after propachlor treatment. We found several GAPDH peptides to be more proteolytically sensitive to proteinase K after propachlor treatment (**Figure 6** and **Figure S13)**, including the active site peptides LVINGNPITIFQER, LISWYDNEFGYSNR, VGVNGFGR. Hence, propachlor induces a more extended conformation in GAPDH, consistent with destabilization. Destabilization of GAPDH could also affect protein-protein interactions. One of the destabilized peptides, VPTANVSVVDLTCR, is involved in the dimer interface of GAPDH[108]. Mutations in this peptide are associated with conformational changes at the dimeric interface and a loss of tetrameric stability[97]. Destabilization of VPTANVSVVDLTCR in GAPDH by propachlor exposure may inhibit the active conformation and affect binding partners. No meaningful change in proteolytic susceptibility was observed for IISNASCTNCLAPLAK, which encompasses the propachlor adduct site. Since this peptide can only be observed in GAPDH that has not been directly modified by propachlor, this implies that the stability of unmodified GAPDH is not generally perturbed by the treatment. We also attempted LiP on PARK7 peptides. Only three peptides proved suitable for LiP (**Table S1**), and none showed evidence of differential proteolytic susceptibility following propachlor treatment (**Figure S13B**). While this indicates that the protein as a whole is not destabilized, it does not exclude the possibility that unprofiled regions of the protein might be affected.

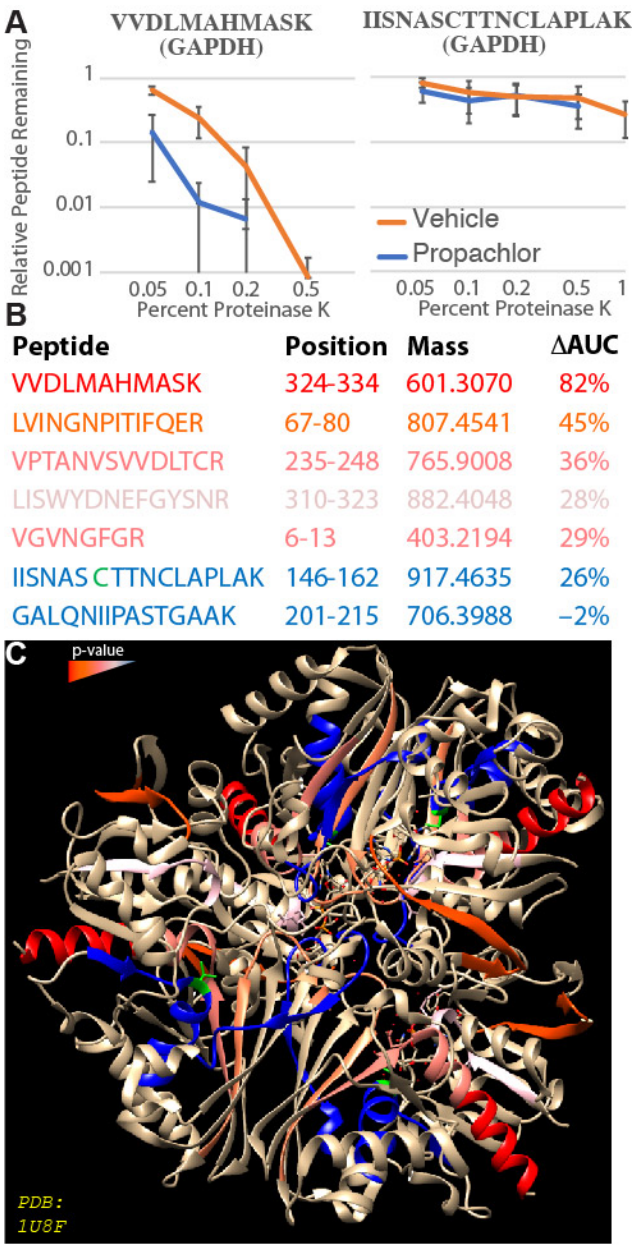

Figure 6: Propachlor destabilization of GAPDH peptides measured by limited proteolysis (LiP). A) LiP-PRM traces illustrating the proteolytic susceptibility of two GAPDH peptides following cellular treatment with propachlor (blue) or vehicle (orange) as indicated. B) Characteristics of the analyzed GAPDH peptides. ΔAUC refers to the decrease in the area under the curve for the proteolytic susceptibility curves. C) The GAPDH peptides are colored according to the significance of the effect of propachlor treatment on proteolytic susceptibility. C152 is indicated in green. The structure (PDB: 1U8F) is taken from Jenkins et al.[109,110]. PRM chromatograms are in **Figure S16**.

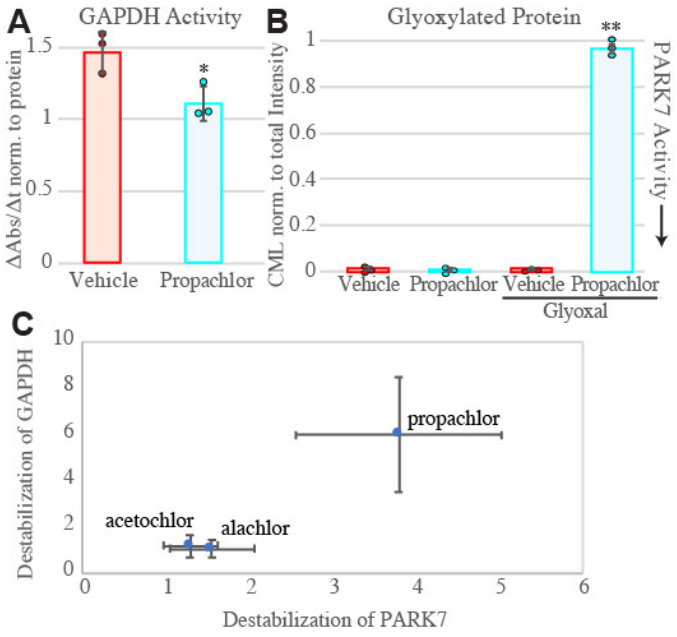

Figure 7: **A**) Activity of GAPDH from cells treated with propachlor or vehicle. Activity was determined from the NADH production rate in lysates, as measured by colorimetry at 450 nm over the linear range, and normalized to total protein (g/mL) as determined by Bradford assay. $p < 0.05$ by Student's two tailed t-test, n = 3). Kinetic traces are in **Figure S14A**. **B**) Inactivation of PARK7 determined by total anti-carboxymethyllysine (CML) densitometry of SDS-PAGE separated lysates. HEK293T cells were treated for 30 min. with vehicle or propachlor (1 mM in serum-free media), followed by 2 h treatment with vehicle or glyoxal (4 mM) and immediate lysis (n = 3). 2-way ANOVA yields F = 1909 > Fcrit = 4.07, and Tukey's HSD finds propachlor + glyoxal condition mean differences compared to all other conditions exceeds the q_{crit} for 0.001. **C**) Relative Hsp40 affinities of GAPDH and PARK7 following the three cellular treatments. Error represents standard deviation. One data point for GAPDH after alachlor treatment was removed as an outlier using Grubb's Test ($G = 2.55 > G_{0.95} = 2.11$, n = 9).

Protein destabilization can lead to both gain-of-function (toxic conformations) and loss-of-function. GAPDH activity has previously been shown to decrease in response to methylglyoxal and copper exposures, presumably due to conjugate and oxidation respectively[35,99]. GAPDH modification can further lead to misfolding and aggregation[111,112]. We evaluated GAPDH activity in cells treated with propachlor. GAPDH activity in lysates was measured using a colorimetric assay for NAD^+ reduction in the presence of substrate. Treating HEK293T cells with 1 mM propachlor for 30

minutes decreased GAPDH activity by 25% (**Figure 7A**). This decrease is consistent with the amount of C152 adducts that we detect by mass spectrometry, but low considering the strong negative cooperativity between the two catalytic sites on the GAPDH tetramer[113]. Our proteomic characterization of propachlor-induced aggregation found an increase in GAPDH aggregation induced by propachlor treatment (FC in aggregates = 4.9, q-value = 0.008; **Figure S7**). Similar results were obtained from Western Blot analysis assessing the levels of GAPDH in the pellet fraction after ultracentrifugation (**Figure S15A**), however there is no significant depletion of total GAPDH (**Figure S15B**). From this we can conclude that although GAPDH destabilization following propachlor treatment does lead to an increase in the aggregated fraction, the total burden of GAPDH aggregation on the cell remains small compared to the high levels of the soluble protein.

PARK7 is a chaperone-like peptidase that can repair proteins damaged by a series of aldehyde products, including methylglyoxal and glyoxal. PARK7 specifically protects GAPDH from cysteine and lysine adducts, including glycerate damage caused by metabolic products generated by GAPDH itself[114,115]. PARK7 is also significantly destabilized after propachlor treatment and thus could be inactive. A cellular assay designed to quantify PARK7 ability to deglycate glyoxal modified proteins in HEK293T cells has been previously established[47]. We measured the ability of endogenous PARK7 to degylcate glyoxal-modified proteins after incubation with 1 mM propachlor for 30 minutes (**Figure 7B** and **Figure S14B,C**). In the presence of propachlor, the intensity of proteins converted to carboxy-methyl-lysine after glyoxal treatment increased significantly in comparison with the control experiment (DMSO vehicle treatment).

Cellular exposure to propachlor inhibits PARK7's ability to deglycate damaged proteins, offering an alternative mechanism by which propachlor exposure can induce protein misfolding beyond direct modification. We speculate that it could be beneficial to the cell that GAPDH is inhibited in concert with PARK7, preventing accumulation of glycating equivalents when the detoxification mechanism is also inhibited. Due to poor reproducibility for profiling the active C106 in PARK7, we were not able to compare whether PARK7^{C106} and GAPDH^{C152} are similarly modified across the range of chloroacetamides investigated in the reported high throughput screen[18]. For the three chloroacetanilides in our present study, however, the relationship holds (**Figure 7C**).

In summary, we present profiles of destabilized proteomes in response to cellular exposure to three chloroacetanilide herbicides. While some proteins are destabilized by each treatment, the overall profiles from each herbicide exposure are unique. About 70% of targeted proteins are known to be subject to haloacetamide conjugation at cysteine, consistent with adducts being the primary mechanism of destabilization, but the extent of destabilization does not correlate with haloacetamides reactivity, reflecting the distinction between conjugation and stability. Hsp40 affinity profiling is an effective assay for determining the effect of environmental toxicants on the cellular proteome, both distinct from and complementary to existing technologies.

Acknowledgements

E. Felix provided technical assistance. This work was supported by the University of California, Riverside and a Society of Analytical Chemists of Pittsburgh Starter Grant. We are grateful to J. Zhou and the Analytical Chemistry Instrumental Facility for

technical assistance with intact protein LC-MS, on instrumentation supported by NSF CHE-1828782.

Supplementary Figures (PDF)

Table S1 (.xlsx): CVs for PRM peptides.

Table S2 (.xlsx): Hsp40 affinity TMT-AP-MS results for acetochlor treatment.

Table S3 (.xlsx): Hsp40 affinity TMT-AP-MS results for alachlor treatment.

Table S4 (.xlsx): Hsp40 affinity TMT-AP-MS results for propachlor treatment.

Table S5 (.xlsx): Identified chloroacetanilide peptide conjugates.

Table S6 (.xlsx): Whole cell and insoluble TMT-MS results following propachlor treatment.

Author Contributions

The manuscript was written through contributions of all authors. All authors have given approval to the final version of the manuscript.

Notes

The authors declare no competing financial interest.

REFERENCES

(1) Shannon, D. A.; Weerapana, E. Covalent Protein Modification: The Current Landscape of Residue-Specific Electrophiles. *Curr Opin Chem Biol* **2015**, *24*, 18–26. https://doi.org/10.1016/j.cbpa.2014.10.021.

(2) Liebler, D. C. Protein Damage by Reactive Electrophiles: Targets and Consequences. *Chem Res Toxicol* **2008**, *21* (1), 117–128. https://doi.org/10.1021/tx700235t.

(3) Ghosh, A. K.; Samanta, I.; Mondal, A.; Liu, W. R. Covalent Inhibition in Drug Discovery. *ChemMedChem* **2019**, *14* (9), 889–906. https://doi.org/10.1002/cmdc.201900107.

(4) Livnat-Levanon, N.; Kevei, É.; Kleifeld, O.; Krutauz, D.; Segref, A.; Rinaldi, T.; Erpapazoglou, Z.; Cohen, M.; Reis, N.; Hoppe, T.; Glickman, M. H. Reversible 26S Proteasome Disassembly upon Mitochondrial Stress. *Cell Rep* **2014**, *7* (5), 1371–1380. https://doi.org/10.1016/j.celrep.2014.04.030.

(5) Allaman, I.; Bélanger, M.; Magistretti, P. J. Methylglyoxal, the Dark Side of Glycolysis. *Front Neurosci* **2015**, *9*, 23. https://doi.org/10.3389/fnins.2015.00023.

(6) Isom, D. G.; Castaneda, C. A.; Cannon, B. R.; Garcia-Moreno E., B. Large Shifts in PKa Values of Lysine Residues Buried inside a Protein. *Proceedings of the National Academy of Sciences* **2011**, *108* (13), 5260–5265. https://doi.org/10.1073/pnas.1010750108.

(7) Mohanty, S. S.; Jena, H. M. A Systemic Assessment of the Environmental Impacts and Remediation Strategies for Chloroacetanilide Herbicides. *Journal of Water Process Engineering* **2019**, *31*, 100860. https://doi.org/10.1016/j.jwpe.2019.100860.

(8) Dearfield, K. L.; McCarroll, N. E.; Protzel, A.; Stack, H. F.; Jackson, M. A.; Waters, M. D. A Survey of EPA/OPP and Open Literature on Selected Pesticide Chemicals. II. Mutagenicity and Carcinogenicity of Selected Chloroacetanilides and Related Compounds. *Mutat Res* **1999**, *443* (1–2), 183–221. https://doi.org/10.1016/s1383-5742(99)00019-8.

(9) Lerro, C. C.; Koutros, S.; Andreotti, G.; Hines, C. J.; Blair, A.; Lubin, J.; Ma, X.; Zhang, Y.; Beane Freeman, L. E. Use of Acetochlor and Cancer Incidence in the Agricultural Health Study: Use of Acetochlor and Cancer Incidence. *Int. J. Cancer* **2015**, *137* (5), 1167–1175. https://doi.org/10.1002/ijc.29416.

(10) Gideon, J.; Mulligan, J.; Hui, C.; Cheng, S.-Y. UV and Temperature Effects on Chloroacetanilide and Triazine Herbicides Degradation and Cytotoxicity. *Heliyon* **2021**, *7* (9), e08010. https://doi.org/10.1016/j.heliyon.2021.e08010.

(11) Atwood, D. *Pesticides Industry Sales and Usage 2008 – 2012 Market Estimates*; Biological and Economic Analysis Division, U.S. Enivornmental Protection Agency, 2017.

(12) Hill, A. B.; Jefferies, P. R.; Quistad, G. B.; Casida, J. E. Dialkylquinoneimine Metabolites of Chloroacetanilide Herbicides Induce Sister Chromatid Exchanges in Cultured Human Lymphocytes. *Mutat Res* **1997**, *395* (2–3), 159–171. https://doi.org/10.1016/s1383-5718(97)00163-0.

(13) Green, T.; Lee, R.; Moore, R. B.; Ashby, J.; Willis, G. A.; Lund, V. J.; Clapp, M. J. L. Acetochlor-Induced Rat Nasal Tumors: Further Studies on the Mode of Action and Relevance to Humans. *Regulatory Toxicology and Pharmacology* **2000**, *32* (1), 127–133. https://doi.org/10.1006/rtph.2000.1413.

(14) Ateeq, B.; Abul Farah, M.; Ahmad, W. Detection of DNA Damage by Alkaline Single Cell Gel Electrophoresis in 2,4-Dichlorophenoxyacetic-Acid- and Butachlor-Exposed Erythrocytes of Clarias Batrachus. *Ecotoxicology and Environmental Safety* **2005**, *62* (3), 348–354. https://doi.org/10.1016/j.ecoenv.2004.12.011.

(15) Ashby, J.; Kier, L.; Wilson, A.; Green, T.; Lefevre, P.; Tinwell, H.; Willis, G.; Heydens, W.; Clapp, M. Evaluation of the Potential Carcinogenicity and Genetic Toxicity to Humans of the Herbicide

Acetochlor. *Hum Exp Toxicol* **1996**, *15* (9), 702–735. https://doi.org/10.1177/096032719601500902.
(16) Counihan, J. L.; Duckering, M.; Dalvie, E.; Ku, W.; Bateman, L. A.; Fisher, K. J.; Nomura, D. K. Chemoproteomic Profiling of Acetanilide Herbicides Reveals Their Role in Inhibiting Fatty Acid Oxidation. *ACS Chem. Biol.* **2017**, *12* (3), 635–642. https://doi.org/10.1021/acschembio.6b01001.
(17) Bateman, L. A.; Nguyen, T. B.; Roberts, A. M.; Miyamoto, D. K.; Ku, W.-M.; Huffman, T. R.; Petri, Y.; Heslin, M. J.; Contreras, C. M.; Skibola, C. F.; Olzmann, J. A.; Nomura, D. K. Chemoproteomics-Enabled Covalent Ligand Screen Reveals a Cysteine Hotspot in Reticulon 4 That Impairs ER Morphology and Cancer Pathogenicity. *Chem. Commun. (Camb.)* **2017**, *53* (53), 7234–7237. https://doi.org/10.1039/c7cc01480e.
(18) Kuljanin, M.; Mitchell, D. C.; Schweppe, D. K.; Gikandi, A. S.; Nusinow, D. P.; Bulloch, N. J.; Vinogradova, E. V.; Wilson, D. L.; Kool, E. T.; Mancias, J. D.; Cravatt, B. F.; Gygi, S. P. Reimagining High-Throughput Profiling of Reactive Cysteines for Cell-Based Screening of Large Electrophile Libraries. *Nat Biotechnol* **2021**, *39* (5), 630–641. https://doi.org/10.1038/s41587-020-00778-3.
(19) Jia, Z.; Misra, H. P. Reactive Oxygen Species in in Vitro Pesticide-Induced Neuronal Cell (SH-SY5Y) Cytotoxicity: Role of NFkappaB and Caspase-3. *Free Radic Biol Med* **2007**, *42* (2), 288–298. https://doi.org/10.1016/j.freeradbiomed.2006.10.047.
(20) Murali, M.; Carvalho, M. S.; Shivanandappa, T. Oxidative Stress-Mediated Cytotoxicity of Endosulfan Is Causally Linked to the Inhibition of NADH Dehydrogenase and Na+, K+-ATPase in Ehrlich Ascites Tumor Cells. *Mol Cell Biochem* **2020**, *468* (1–2), 59–68. https://doi.org/10.1007/s11010-020-03711-z.
(21) Castello, P. R.; Drechsel, D. A.; Patel, M. Mitochondria Are a Major Source of Paraquat-Induced Reactive Oxygen Species Production in the Brain. *Journal of Biological Chemistry* **2007**, *282* (19), 14186–14193. https://doi.org/10.1074/jbc.M700827200.
(22) Manning-Bog, A. B.; McCormack, A. L.; Li, J.; Uversky, V. N.; Fink, A. L.; Di Monte, D. A. The Herbicide Paraquat Causes Up-Regulation and Aggregation of α-Synuclein in Mice: PARAQUAT AND α-SYNUCLEIN. *J. Biol. Chem.* **2002**, *277* (3), 1641–1644. https://doi.org/10.1074/jbc.C100560200.
(23) Lafon, P.-A.; Imberdis, T.; Wang, Y.; Torrent, J.; Robitzer, M.; Huetter, E.; Alvarez-Martinez, M.-T.; Chevallier, N.; Givalois, L.; Desrumaux, C.; Liu, J.; Perrier, V. Low Doses of Bioherbicide Favour Prion Aggregation and Propagation in Vivo. *Sci Rep* **2018**, *8* (1), 8023. https://doi.org/10.1038/s41598-018-25966-9.
(24) Devi, S.; Karsauliya, K.; Srivastava, T.; Raj, R.; Kumar, D.; Priya, S. Pesticide Interactions Induce Alterations in Secondary Structure of Malate Dehydrogenase to Cause Destability and Cytotoxicity. *Chemosphere* **2021**, *263*, 128074. https://doi.org/10.1016/j.chemosphere.2020.128074.
(25) Devi, S.; Chaturvedi, M.; Fatima, S.; Priya, S. Environmental Factors Modulating Protein Conformations and Their Role in Protein Aggregation Diseases. *Toxicology* **2022**, *465*, 153049. https://doi.org/10.1016/j.tox.2021.153049.
(26) Santra, M.; Dill, K. A.; de Graff, A. M. R. Proteostasis Collapse Is a Driver of Cell Aging and Death. *Proc Natl Acad Sci USA* **2019**, *116* (44), 22173–22178. https://doi.org/10.1073/pnas.1906592116.
(27) Yu, A.; Shibata, Y.; Shah, B.; Calamini, B.; Lo, D. C.; Morimoto, R. I. Protein Aggregation Can Inhibit Clathrin-Mediated Endocytosis by Chaperone Competition. *Proc. Natl. Acad. Sci. U.S.A.* **2014**, *111* (15), E1481-1490. https://doi.org/10.1073/pnas.1321811111.
(28) Gidalevitz, T.; Prahlad, V.; Morimoto, R. I. The Stress of Protein Misfolding: From Single Cells to Multicellular Organisms. *Cold Spring Harbor Perspectives in Biology* **2011**, *3* (6), a009704–a009704. https://doi.org/10.1101/cshperspect.a009704.

(29) Kaur, U.; Meng, H.; Lui, F.; Ma, R.; Ogburn, R. N.; Johnson, J. H. R.; Fitzgerald, M. C.; Jones, L. M. Proteome-Wide Structural Biology: An Emerging Field for the Structural Analysis of Proteins on the Proteomic Scale. *Journal of Proteome Research* **2018**, *17* (11), 3614–3627.
(30) McKenzie-Coe, A.; Montes, N. S.; Jones, L. M. Hydroxyl Radical Protein Footprinting: A Mass Spectrometry-Based Structural Method for Studying the Higher Order Structure of Proteins. *Chem. Rev.* **2022**, *122* (8), 7532–7561. https://doi.org/10.1021/acs.chemrev.1c00432.
(31) Ma, R.; Meng, H.; Wiebelhaus, N.; Fitzgerald, M. C. Chemo-Selection Strategy for Limited Proteolysis Experiments on the Proteomic Scale. *Anal. Chem.* **2018**, *90* (23), 14039–14047. https://doi.org/10.1021/acs.analchem.8b04122.
(32) Bamberger, C.; Pankow, S.; Martínez-Bartolomé, S.; Ma, M.; Diedrich, J.; Rissman, R. A.; Yates, J. R. Protein Footprinting via Covalent Protein Painting Reveals Structural Changes of the Proteome in Alzheimer's Disease. *J Proteome Res* **2021**, *20* (5), 2762–2771. https://doi.org/10.1021/acs.jproteome.0c00912.
(33) Schopper, S.; Kahraman, A.; Leuenberger, P.; Feng, Y.; Piazza, I.; Müller, O.; Boersema, P. J.; Picotti, P. Measuring Protein Structural Changes on a Proteome-Wide Scale Using Limited Proteolysis-Coupled Mass Spectrometry. *Nat Protoc* **2017**, *12* (11), 2391–2410. https://doi.org/10.1038/nprot.2017.100.
(34) Cox, D.; Ang, C.-S.; Nillegoda, N. B.; Reid, G. E.; Hatters, D. M. Hidden Information on Protein Function in Censuses of Proteome Foldedness. *Nat Commun* **2022**, *13* (1), 1992. https://doi.org/10.1038/s41467-022-29661-2.
(35) Wiebelhaus, N.; Zaengle-Barone, J. M.; Hwang, K. K.; Franz, K. J.; Fitzgerald, M. C. Protein Folding Stability Changes Across the Proteome Reveal Targets of Cu Toxicity in *E. Coli*. *ACS Chem. Biol.* **2021**, *16* (1), 214–224. https://doi.org/10.1021/acschembio.0c00900.
(36) Geer Wallace, M. A.; Kwon, D.-Y.; Weitzel, D. H.; Lee, C.-T.; Stephenson, T. N.; Chi, J.-T.; Mook, R. A.; Dewhirst, M. W.; Hong, J.; Fitzgerald, M. C. Discovery of Manassantin A Protein Targets Using Large-Scale Protein Folding and Stability Measurements. *J. Proteome Res.* **2016**, *15* (8), 2688–2696. https://doi.org/10.1021/acs.jproteome.6b00237.
(37) Quanrud, G. M.; Montoya, M. R.; Mei, L.; Awad, M. R.; Genereux, J. C. Hsp40 Affinity to Identify Proteins Destabilized by Cellular Toxicant Exposure. *Anal Chem* **2021**, *93* (50), 16940–16946. https://doi.org/10.1021/acs.analchem.1c04230.
(38) Mei, L.; Montoya, M. R.; Quanrud, G. M.; Tran, M.; Villa-Sharma, A.; Huang, M.; Genereux, J. C. Bait Correlation Improves Interactor Identification by Tandem Mass Tag-Affinity Purification-Mass Spectrometry. *J. Proteome Res.* **2020**, *19* (4), 1565–1573. https://doi.org/10.1021/acs.jproteome.9b00825.
(39) Montoya, M. R.; Quanrud, G. M.; Mei, L.; Montaño, J. L.; Genereux, J. C. *Evaluating Client Protein Recovery by the Hsp40s DNAJB8 and DNAJB1 with AP-MS*; preprint; bioRxiv, 2022. https://doi.org/10.1101/2022.03.31.485989.
(40) Washburn, M. P.; Wolters, D.; Yates, J. R. Large-Scale Analysis of the Yeast Proteome by Multidimensional Protein Identification Technology. *Nat Biotechnol* **2001**, *19* (3), 242–247. https://doi.org/10.1038/85686.
(41) Kong, A. T.; Leprevost, F. V.; Avtonomov, D. M.; Mellacheruvu, D.; Nesvizhskii, A. I. MSFragger: Ultrafast and Comprehensive Peptide Identification in Mass Spectrometry–Based Proteomics. *Nat Methods* **2017**, *14* (5), 513–520. https://doi.org/10.1038/nmeth.4256.
(42) Yu, F.; Teo, G. C.; Kong, A. T.; Haynes, S. E.; Avtonomov, D. M.; Geiszler, D. J.; Nesvizhskii, A. I. Identification of Modified Peptides Using Localization-Aware Open Search. *Nat Commun* **2020**, *11* (1), 4065. https://doi.org/10.1038/s41467-020-17921-y.
(43) Plubell, D. L.; Wilmarth, P. A.; Zhao, Y.; Fenton, A. M.; Minnier, J.; Reddy, A. P.; Klimek, J.; Yang, X.; David, L. L.; Pamir, N. Extended Multiplexing of Tandem Mass Tags (TMT) Labeling Reveals Age

and High Fat Diet Specific Proteome Changes in Mouse Epididymal Adipose Tissue. *Mol Cell Proteomics* **2017**, *16* (5), 873–890. https://doi.org/10.1074/mcp.M116.065524.
(44) Yekutieli, D.; Benjamini, Y. Resampling-Based False Discovery Rate Controlling Multiple Test Procedures for Correlated Test Statistics. *Journal of Statistical Planning and Inference* **1999**, *82* (1–2), 171–196. https://doi.org/10.1016/S0378-3758(99)00041-5.
(45) Storey, J. D.; Tibshirani, R. Statistical Significance for Genomewide Studies. *Proceedings of the National Academy of Sciences of the United States of America* **2003**, *100* (16), 9440–9445.
(46) MacLean, B.; Tomazela, D. M.; Shulman, N.; Chambers, M.; Finney, G. L.; Frewen, B.; Kern, R.; Tabb, D. L.; Liebler, D. C.; MacCoss, M. J. Skyline: An Open Source Document Editor for Creating and Analyzing Targeted Proteomics Experiments. *Bioinformatics* **2010**, *26* (7), 966–968.
(47) Tashiro, S.; Caaveiro, J. M. M.; Nakakido, M.; Tanabe, A.; Nagatoishi, S.; Tamura, Y.; Matsuda, N.; Liu, D.; Hoang, Q. Q.; Tsumoto, K. Discovery and Optimization of Inhibitors of the Parkinson's Disease Associated Protein DJ-1. *ACS Chem. Biol.* **2018**, *13* (9), 2783–2793. https://doi.org/10.1021/acschembio.8b00701.
(48) Cao, S. S.; Kaufman, R. J. Endoplasmic Reticulum Stress and Oxidative Stress in Cell Fate Decision and Human Disease. *Antioxid Redox Signal* **2014**, *21* (3), 396–413. https://doi.org/10.1089/ars.2014.5851.
(49) Anckar, J.; Sistonen, L. Regulation of HSF1 Function in the Heat Stress Response: Implications in Aging and Disease. *Annu Rev Biochem* **2011**, *80*, 1089–1115. https://doi.org/10.1146/annurev-biochem-060809-095203.
(50) Lambert, G. R.; Padgett, W. T.; George, M. H.; Kitchin, K. T.; Nesnow, S. Quantitative Analysis of Alachlor Protein Adducts by Gas Chromatography–Mass Spectrometry. *Analytical Biochemistry* **1999**, *268* (2), 289–296. https://doi.org/10.1006/abio.1998.3060.
(51) Liu, X.; Ling, Z.; Zhou, X.; Ahmad, F.; Zhou, Y. Comprehensive Spectroscopic Probing the Interaction and Conformation Impairment of Bovine Serum Albumin (BSA) by Herbicide Butachlor. *Journal of Photochemistry and Photobiology B: Biology* **2016**, *162*, 332–339. https://doi.org/10.1016/j.jphotobiol.2016.07.005.
(52) Gillis, J.; Schipper-Krom, S.; Juenemann, K.; Gruber, A.; Coolen, S.; van den Nieuwendijk, R.; van Veen, H.; Overkleeft, H.; Goedhart, J.; Kampinga, H. H.; Reits, E. A. The DNAJB6 and DNAJB8 Protein Chaperones Prevent Intracellular Aggregation of Polyglutamine Peptides. *J. Biol. Chem.* **2013**, *288* (24), 17225–17237. https://doi.org/10.1074/jbc.M112.421685.
(53) Hageman, J.; Rujano, M. A.; van Waarde, M. A. W. H.; Kakkar, V.; Dirks, R. P.; Govorukhina, N.; Oosterveld-Hut, H. M. J.; Lubsen, N. H.; Kampinga, H. H. A DNAJB Chaperone Subfamily with HDAC-Dependent Activities Suppresses Toxic Protein Aggregation. *Molecular Cell* **2010**, *37* (3), 355–369. https://doi.org/10.1016/j.molcel.2010.01.001.
(54) Kakkar, V.; Månsson, C.; de Mattos, E. P.; Bergink, S.; van der Zwaag, M.; van Waarde, M. A. W. H.; Kloosterhuis, N. J.; Melki, R.; van Cruchten, R. T. P.; Al-Karadaghi, S.; Arosio, P.; Dobson, C. M.; Knowles, T. P. J.; Bates, G. P.; van Deursen, J. M.; Linse, S.; van de Sluis, B.; Emanuelsson, C.; Kampinga, H. H. The S/T-Rich Motif in the DNAJB6 Chaperone Delays Polyglutamine Aggregation and the Onset of Disease in a Mouse Model. *Molecular Cell* **2016**, *62* (2), 272–283. https://doi.org/10.1016/j.molcel.2016.03.017.
(55) Powers, E. T.; Gierasch, L. M. The Proteome Folding Problem and Cellular Proteostasis. *Journal of Molecular Biology* **2021**, *433* (20), 167197. https://doi.org/10.1016/j.jmb.2021.167197.
(56) Rauniyar, N.; Yates, J. R. Isobaric Labeling-Based Relative Quantification in Shotgun Proteomics. *J Proteome Res* **2014**, *13* (12), 5293–5309. https://doi.org/10.1021/pr500880b.
(57) Carreras, C. W.; Santi, D. V. THE CATALYTIC MECHANISM AND STRUCTURE OF THYMIDYLATE SYNTHASE. *Annu. Rev. Biochem.* **1995**, *64* (1), 721–762. https://doi.org/10.1146/annurev.bi.64.070195.003445.

(58) Hyatt, D. C.; Maley, F.; Montfort, W. R. Use of Strain in a Stereospecific Catalytic Mechanism: Crystal Structures of *Escherichia Coli* Thymidylate Synthase Bound to FdUMP and Methylenetetrahydrofolate′. *Biochemistry* **1997**, *36* (15), 4585–4594. https://doi.org/10.1021/bi962936j.
(59) Sesen, J.; Cammas, A.; Scotland, S. J.; Elefterion, B.; Lemarié, A.; Millevoi, S.; Mathew, L. K.; Seva, C.; Toulas, C.; Moyal, E. C.-J.; Skuli, N. Int6/EIF3e Is Essential for Proliferation and Survival of Human Glioblastoma Cells. *Int J Mol Sci* **2014**, *15* (2), 2172–2190. https://doi.org/10.3390/ijms15022172.
(60) Guo, Z.-Y.; Chang, C. C. Y.; Chang, T.-Y. Functionality of the Seventh and Eighth Transmembrane Domains of Acyl-Coenzyme A:Cholesterol Acyltransferase 1. *Biochemistry* **2007**, *46* (35), 10063–10071. https://doi.org/10.1021/bi7011367.
(61) Weerapana, E.; Wang, C.; Simon, G. M.; Richter, F.; Khare, S.; Dillon, M. B. D.; Bachovchin, D. A.; Mowen, K.; Baker, D.; Cravatt, B. F. Quantitative Reactivity Profiling Predicts Functional Cysteines in Proteomes. *Nature* **2010**, *468* (7325), 790–795. https://doi.org/10.1038/nature09472.
(62) Kuang, Q.; Purhonen, P.; Ålander, J.; Svensson, R.; Hoogland, V.; Winerdal, J.; Spahiu, L.; Ottosson-Wadlund, A.; Jegerschöld, C.; Morgenstern, R.; Hebert, H. Dead-End Complex, Lipid Interactions and Catalytic Mechanism of Microsomal Glutathione Transferase 1, an Electron Crystallography and Mutagenesis Investigation. *Sci Rep* **2017**, *7* (1), 7897. https://doi.org/10.1038/s41598-017-07912-3.
(63) Horibata, Y.; Ando, H.; Sugimoto, H. Locations and Contributions of the Phosphotransferases EPT1 and CEPT1 to the Biosynthesis of Ethanolamine Phospholipids. *J Lipid Res* **2020**, *61* (8), 1221–1231. https://doi.org/10.1194/jlr.RA120000898.
(64) Dörrbaum, A. R.; Kochen, L.; Langer, J. D.; Schuman, E. M. Local and Global Influences on Protein Turnover in Neurons and Glia. *eLife* **2018**, *7*, e34202. https://doi.org/10.7554/eLife.34202.
(65) Li, J.; Cai, Z.; Vaites, L. P.; Shen, N.; Mitchell, D. C.; Huttlin, E. L.; Paulo, J. A.; Harry, B. L.; Gygi, S. P. Proteome-Wide Mapping of Short-Lived Proteins in Human Cells. *Molecular Cell* **2021**, *81* (22), 4722-4735.e5. https://doi.org/10.1016/j.molcel.2021.09.015.
(66) Marzec, K.; Burgess, A. The Oncogenic Functions of MASTL Kinase. *Front. Cell Dev. Biol.* **2018**, *6*, 162. https://doi.org/10.3389/fcell.2018.00162.
(67) Jia, D.; Hasso, S. M.; Chan, J.; Filingeri, D.; D'Amore, P. A.; Rice, L.; Pampo, C.; Siemann, D. W.; Zurakowski, D.; Rodig, S. J.; Moses, M. A. Transcriptional Repression of VEGF by ZNF24: Mechanistic Studies and Vascular Consequences in Vivo. *Blood* **2013**, *121* (4), 707–715. https://doi.org/10.1182/blood-2012-05-433045.
(68) Anwair, M. A. S.; Károlyházy, L.; Szabó, D.; Balogh, B.; Kövesdi, I.; Harmat, V.; Krenyácz, J.; Gellért, Á.; Takács-Novák, K.; Mátyus, P. Lipophilicity of Aminopyridazinone Regioisomers. *J. Agric. Food Chem.* **2003**, *51* (18), 5262–5270. https://doi.org/10.1021/jf0343938.
(69) Shannon, D. A.; Banerjee, R.; Webster, E. R.; Bak, D. W.; Wang, C.; Weerapana, E. Investigating the Proteome Reactivity and Selectivity of Aryl Halides. *J. Am. Chem. Soc.* **2014**, *136* (9), 3330–3333. https://doi.org/10.1021/ja4116204.
(70) Coleman, S.; Linderman, R.; Hodgson, E.; Rose, R. L. Comparative Metabolism of Chloroacetamide Herbicides and Selected Metabolites in Human and Rat Liver Microsomes. *Environ. Health Perspect.* **2000**, *108* (12), 1151–1157. https://doi.org/10.1289/ehp.001081151.
(71) Bonfanti, M.; Taverna, P.; Chiappetta, L.; Villa, P.; D'Incalci, M.; Bagnati, R.; Fanelli, R. DNA Damage Induced by Alachlor after in Vitro Activation by Rat Hepatocytes. *Toxicology* **1992**, *72* (2), 207–219. https://doi.org/10.1016/0300-483X(92)90113-S.
(72) Seidler, N. W. *GAPDH: Biological Properties and Diversity*; Advances in Experimental Medicine and Biology; Springer Netherlands: Dordrecht, 2013; Vol. 985. https://doi.org/10.1007/978-94-007-4716-6.

(73) Sirover, M. A. On the Functional Diversity of Glyceraldehyde-3-Phosphate Dehydrogenase: Biochemical Mechanisms and Regulatory Control. *Biochimica et Biophysica Acta (BBA) - General Subjects* **2011**, *1810* (8), 741–751. https://doi.org/10.1016/j.bbagen.2011.05.010.
(74) Jung, Y.; Noda, N.; Takaya, J.; Abo, M.; Toh, K.; Tajiri, K.; Cui, C.; Zhou, L.; Sato, S.; Uesugi, M. Discovery of Non-Cysteine-Targeting Covalent Inhibitors by Activity-Based Proteomic Screening with a Cysteine-Reactive Probe. *ACS Chem. Biol.* **2022**, *17* (2), 340–347. https://doi.org/10.1021/acschembio.1c00824.
(75) Hall, D. R.; Yeung, K.; Peng, H. Monohaloacetic Acids and Monohaloacetamides Attack Distinct Cellular Proteome Thiols. *Environ. Sci. Technol.* **2020**, *54* (23), 15191–15201. https://doi.org/10.1021/acs.est.0c03144.
(76) Vanle, B. C.; Florang, V. R.; Murry, D. J.; Aguirre, A. L.; Doorn, J. A. Inactivation of Glyceraldehyde-3-Phosphate Dehydrogenase by the Dopamine Metabolite, 3,4-Dihydroxyphenylacetaldehyde. *Biochem Biophys Res Commun* **2017**, *492* (2), 275–281. https://doi.org/10.1016/j.bbrc.2017.08.067.
(77) Repici, M.; Giorgini, F. DJ-1 in Parkinson's Disease: Clinical Insights and Therapeutic Perspectives. *JCM* **2019**, *8* (9), 1377. https://doi.org/10.3390/jcm8091377.
(78) Liu, F.; Nguyen, J. L.; Hulleman, J. D.; Li, L.; Rochet, J.-C. Mechanisms of DJ-1 Neuroprotection in a Cellular Model of Parkinson's Disease: Mechanisms of Neuroprotection by DJ-1. *Journal of Neurochemistry* **2008**, *105* (6), 2435–2453. https://doi.org/10.1111/j.1471-4159.2008.05333.x.
(79) Dolgacheva, L. P.; Berezhnov, A. V.; Fedotova, E. I.; Zinchenko, V. P.; Abramov, A. Y. Role of DJ-1 in the Mechanism of Pathogenesis of Parkinson's Disease. *J Bioenerg Biomembr* **2019**, *51* (3), 175–188. https://doi.org/10.1007/s10863-019-09798-4.
(80) Lippa, K. A.; Demel, S.; Lau, I. H.; Roberts, A. L. Kinetics and Mechanism of the Nucleophilic Displacement Reactions of Chloroacetanilide Herbicides: Investigation of α-Substituent Effects. *J. Agric. Food Chem.* **2004**, *52* (10), 3010–3021. https://doi.org/10.1021/jf030290d.
(81) Ward, C. C.; Kleinman, J. I.; Nomura, D. K. NHS-Esters As Versatile Reactivity-Based Probes for Mapping Proteome-Wide Ligandable Hotspots. *ACS Chem. Biol.* **2017**, *12* (6), 1478–1483. https://doi.org/10.1021/acschembio.7b00125.
(82) Ford, B.; Bateman, L. A.; Gutierrez-Palominos, L.; Park, R.; Nomura, D. K. Mapping Proteome-Wide Targets of Glyphosate in Mice. *Cell Chem Biol* **2017**, *24* (2), 133–140. https://doi.org/10.1016/j.chembiol.2016.12.013.
(83) Chen, W.; Dong, J.; Plate, L.; Mortenson, D. E.; Brighty, G. J.; Li, S.; Liu, Y.; Galmozzi, A.; Lee, P. S.; Hulce, J. J.; Cravatt, B. F.; Saez, E.; Powers, E. T.; Wilson, I. A.; Sharpless, K. B.; Kelly, J. W. Arylfluorosulfates Inactivate Intracellular Lipid Binding Protein(s) through Chemoselective SuFEx Reaction with a Binding Site Tyr Residue. *J. Am. Chem. Soc.* **2016**, *138* (23), 7353–7364. https://doi.org/10.1021/jacs.6b02960.
(84) Fert-Bober, J.; Murray, C. I.; Parker, S. J.; Van Eyk, J. E. Precision Profiling of the Cardiovascular Post-Translationally Modified Proteome: Where There Is a Will, There Is a Way. *Circ Res* **2018**, *122* (9), 1221–1237. https://doi.org/10.1161/CIRCRESAHA.118.310966.
(85) Jeong, K.; Kim, S.; Bandeira, N. False Discovery Rates in Spectral Identification. *BMC Bioinformatics* **2012**, *13 Suppl 16*, S2. https://doi.org/10.1186/1471-2105-13-S16-S2.
(86) Anapindi, K. D. B.; Romanova, E. V.; Southey, B. R.; Sweedler, J. V. Peptide Identifications and False Discovery Rates Using Different Mass Spectrometry Platforms. *Talanta* **2018**, *182*, 456–463. https://doi.org/10.1016/j.talanta.2018.01.062.
(87) Ryder, B. D.; Matlahov, I.; Bali, S.; Vaquer-Alicea, J.; van der Wel, P. C. A.; Joachimiak, L. A. Regulatory Inter-Domain Interactions Influence Hsp70 Recruitment to the DnaJB8 Chaperone. *Nat Commun* **2021**, *12* (1), 946. https://doi.org/10.1038/s41467-021-21147-x.

(88) Radford, S. E.; Dobson, C. M.; Evans, P. A. The Folding of Hen Lysozyme Involves Partially Structured Intermediates and Multiple Pathways. *Nature* **1992**, *358* (6384), 302–307. https://doi.org/10.1038/358302a0.
(89) Colon, W.; Kelly, J. W. Partial Denaturation of Transthyretin Is Sufficient for Amyloid Fibril Formation in Vitro. *Biochemistry* **1992**, *31* (36), 8654–8660. https://doi.org/10.1021/bi00151a036.
(90) Baldwin, A. J.; Knowles, T. P. J.; Tartaglia, G. G.; Fitzpatrick, A. W.; Devlin, G. L.; Shammas, S. L.; Waudby, C. A.; Mossuto, M. F.; Meehan, S.; Gras, S. L.; Christodoulou, J.; Anthony-Cahill, S. J.; Barker, P. D.; Vendruscolo, M.; Dobson, C. M. Metastability of Native Proteins and the Phenomenon of Amyloid Formation. *J. Am. Chem. Soc.* **2011**, *133* (36), 14160–14163. https://doi.org/10.1021/ja2017703.
(91) Sui, X.; Pires, D. E. V.; Ormsby, A. R.; Cox, D.; Nie, S.; Vecchi, G.; Vendruscolo, M.; Ascher, D. B.; Reid, G. E.; Hatters, D. M. Widespread Remodeling of Proteome Solubility in Response to Different Protein Homeostasis Stresses. *Proc Natl Acad Sci U S A* **2020**, *117* (5), 2422–2431. https://doi.org/10.1073/pnas.1912897117.
(92) Kaksonen, M.; Roux, A. Mechanisms of Clathrin-Mediated Endocytosis. *Nat Rev Mol Cell Biol* **2018**, *19* (5), 313–326. https://doi.org/10.1038/nrm.2017.132.
(93) Natsume, W.; Tanabe, K.; Kon, S.; Yoshida, N.; Watanabe, T.; Torii, T.; Satake, M. SMAP2, a Novel ARF GTPase-Activating Protein, Interacts with Clathrin and Clathrin Assembly Protein and Functions on the AP-1-Positive Early Endosome/Trans-Golgi Network. *Mol Biol Cell* **2006**, *17* (6), 2592–2603. https://doi.org/10.1091/mbc.e05-10-0909.
(94) He, K.; Song, E.; Upadhyayula, S.; Dang, S.; Gaudin, R.; Skillern, W.; Bu, K.; Capraro, B. R.; Rapoport, I.; Kusters, I.; Ma, M.; Kirchhausen, T. Dynamics of Auxilin 1 and GAK in Clathrin-Mediated Traffic. *J Cell Biol* **2020**, *219* (3), e201908142. https://doi.org/10.1083/jcb.201908142.
(95) Weids, A. J.; Ibstedt, S.; Tamás, M. J.; Grant, C. M. Distinct Stress Conditions Result in Aggregation of Proteins with Similar Properties. *Sci Rep* **2016**, *6* (1), 24554. https://doi.org/10.1038/srep24554.
(96) Galván-Peña, S.; Carroll, R. G.; Newman, C.; Hinchy, E. C.; Palsson-McDermott, E.; Robinson, E. K.; Covarrubias, S.; Nadin, A.; James, A. M.; Haneklaus, M.; Carpenter, S.; Kelly, V. P.; Murphy, M. P.; Modis, L. K.; O'Neill, L. A. Malonylation of GAPDH Is an Inflammatory Signal in Macrophages. *Nat Commun* **2019**, *10* (1), 338. https://doi.org/10.1038/s41467-018-08187-6.
(97) Qvit, N.; Joshi, A. U.; Cunningham, A. D.; Ferreira, J. C. B.; Mochly-Rosen, D. Glyceraldehyde-3-Phosphate Dehydrogenase (GAPDH) Protein-Protein Interaction Inhibitor Reveals a Non-Catalytic Role for GAPDH Oligomerization in Cell Death. *Journal of Biological Chemistry* **2016**, *291* (26), 13608–13621. https://doi.org/10.1074/jbc.M115.711630.
(98) Uchida, K.; Stadtman, E. R. Covalent Attachment of 4-Hydroxynonenal to Glyceraldehyde-3-Phosphate Dehydrogenase. A Possible Involvement of Intra- and Intermolecular Cross-Linking Reaction. *J Biol Chem* **1993**, *268* (9), 6388–6393.
(99) Lee, H. J.; Howell, S. K.; Sanford, R. J.; Beisswenger, P. J. Methylglyoxal Can Modify GAPDH Activity and Structure. *Ann N Y Acad Sci* **2005**, *1043*, 135–145. https://doi.org/10.1196/annals.1333.017.
(100) Kornberg, M. D.; Bhargava, P.; Kim, P. M.; Putluri, V.; Snowman, A. M.; Putluri, N.; Calabresi, P. A.; Snyder, S. H. Dimethyl Fumarate Targets GAPDH and Aerobic Glycolysis to Modulate Immunity. *Science* **2018**, *360* (6387), 449–453. https://doi.org/10.1126/science.aan4665.
(101) Blatnik, M.; Thorpe, S. R.; Baynes, J. W. Succination of Proteins by Fumarate: Mechanism of Inactivation of Glyceraldehyde-3-Phosphate Dehydrogenase in Diabetes. *Ann N Y Acad Sci* **2008**, *1126*, 272–275. https://doi.org/10.1196/annals.1433.047.
(102) Zambaldo, C.; Vinogradova, E. V.; Qi, X.; Iaconelli, J.; Suciu, R. M.; Koh, M.; Senkane, K.; Chadwick, S. R.; Sanchez, B. B.; Chen, J. S.; Chatterjee, A. K.; Liu, P.; Schultz, P. G.; Cravatt, B. F.; Bollong, M.

J. 2-Sulfonylpyridines as Tunable, Cysteine-Reactive Electrophiles. *J. Am. Chem. Soc.* **2020**, *142* (19), 8972–8979. https://doi.org/10.1021/jacs.0c02721.
(103) Peralta, D.; Bronowska, A. K.; Morgan, B.; Dóka, É.; Van Laer, K.; Nagy, P.; Gräter, F.; Dick, T. P. A Proton Relay Enhances H2O2 Sensitivity of GAPDH to Facilitate Metabolic Adaptation. *Nat Chem Biol* **2015**, *11* (2), 156–163. https://doi.org/10.1038/nchembio.1720.
(104) Park, C.; Marqusee, S. Pulse Proteolysis: A Simple Method for Quantitative Determination of Protein Stability and Ligand Binding. *Nat. Methods* **2005**, *2* (3), 207–212. https://doi.org/10.1038/nmeth740.
(105) Feng, Y.; De Franceschi, G.; Kahraman, A.; Soste, M.; Melnik, A.; Boersema, P. J.; de Laureto, P. P.; Nikolaev, Y.; Oliveira, A. P.; Picotti, P. Global Analysis of Protein Structural Changes in Complex Proteomes. *Nat Biotechnol* **2014**, *32* (10), 1036–1044. https://doi.org/10.1038/nbt.2999.
(106) To, P.; Whitehead, B.; Tarbox, H. E.; Fried, S. D. Nonrefoldability Is Pervasive Across the *E. Coli* Proteome. *J. Am. Chem. Soc.* **2021**, *143* (30), 11435–11448. https://doi.org/10.1021/jacs.1c03270.
(107) Leuenberger, P.; Ganscha, S.; Kahraman, A.; Cappelletti, V.; Boersema, P. J.; von Mering, C.; Claassen, M.; Picotti, P. Cell-Wide Analysis of Protein Thermal Unfolding Reveals Determinants of Thermostability. *Science* **2017**, *355* (6327), eaai7825. https://doi.org/10.1126/science.aai7825.
(108) White, M. R.; Khan, M. M.; Deredge, D.; Ross, C. R.; Quintyn, R.; Zucconi, B. E.; Wysocki, V. H.; Wintrode, P. L.; Wilson, G. M.; Garcin, E. D. A Dimer Interface Mutation in Glyceraldehyde-3-Phosphate Dehydrogenase Regulates Its Binding to AU-Rich RNA. *Journal of Biological Chemistry* **2015**, *290* (3), 1770–1785. https://doi.org/10.1074/jbc.M114.618165.
(109) Jenkins, J. L.; Tanner, J. J. High-Resolution Structure of Human D -Glyceraldehyde-3-Phosphate Dehydrogenase. *Acta Crystallogr D Biol Crystallogr* **2006**, *62* (3), 290–301. https://doi.org/10.1107/S0907444905042289.
(110) Pettersen, E. F.; Goddard, T. D.; Huang, C. C.; Couch, G. S.; Greenblatt, D. M.; Meng, E. C.; Ferrin, T. E. UCSF Chimera--a Visualization System for Exploratory Research and Analysis. *J Comput Chem* **2004**, *25* (13), 1605–1612. https://doi.org/10.1002/jcc.20084.
(111) Zaffagnini, M.; Fermani, S.; Costa, A.; Lemaire, S. D.; Trost, P. Plant Cytoplasmic GAPDH: Redox Post-Translational Modifications and Moonlighting Properties. *Front. Plant Sci.* **2013**, *4*. https://doi.org/10.3389/fpls.2013.00450.
(112) Gerszon, J.; Rodacka, A. Oxidatively Modified Glyceraldehyde-3-Phosphate Dehydrogenase in Neurodegenerative Processes and the Role of Low Molecular Weight Compounds in Counteracting Its Aggregation and Nuclear Translocation. *Ageing Research Reviews* **2018**, *48*, 21–31. https://doi.org/10.1016/j.arr.2018.09.003.
(113) Henis, Y. I.; Levitzki, A. Mechanism of Negative Cooperativity in Glyceraldehyde-3-Phosphate Dehydrogenase Deduced from Ligand Competition Experiments. *Proc Natl Acad Sci U S A* **1980**, *77* (9), 5055–5059. https://doi.org/10.1073/pnas.77.9.5055.
(114) Richarme, G.; Mihoub, M.; Dairou, J.; Bui, L. C.; Leger, T.; Lamouri, A. Parkinsonism-Associated Protein DJ-1/Park7 Is a Major Protein Deglycase That Repairs Methylglyoxal- and Glyoxal-Glycated Cysteine, Arginine, and Lysine Residues. *Journal of Biological Chemistry* **2015**, *290* (3), 1885–1897. https://doi.org/10.1074/jbc.M114.597815.
(115) Heremans, I. P.; Caligiore, F.; Gerin, I.; Bury, M.; Lutz, M.; Graff, J.; Stroobant, V.; Vertommen, D.; Teleman, A. A.; Van Schaftingen, E.; Bommer, G. T. Parkinson's Disease Protein PARK7 Prevents Metabolite and Protein Damage Caused by a Glycolytic Metabolite. *Proc. Natl. Acad. Sci. U.S.A.* **2022**, *119* (4), e2111338119. https://doi.org/10.1073/pnas.2111338119.